Cell Reports

Article

FUS ALS neurons activate major stress pathways and reduce translation as an early protective mechanism against neurodegeneration

Graphical abstract

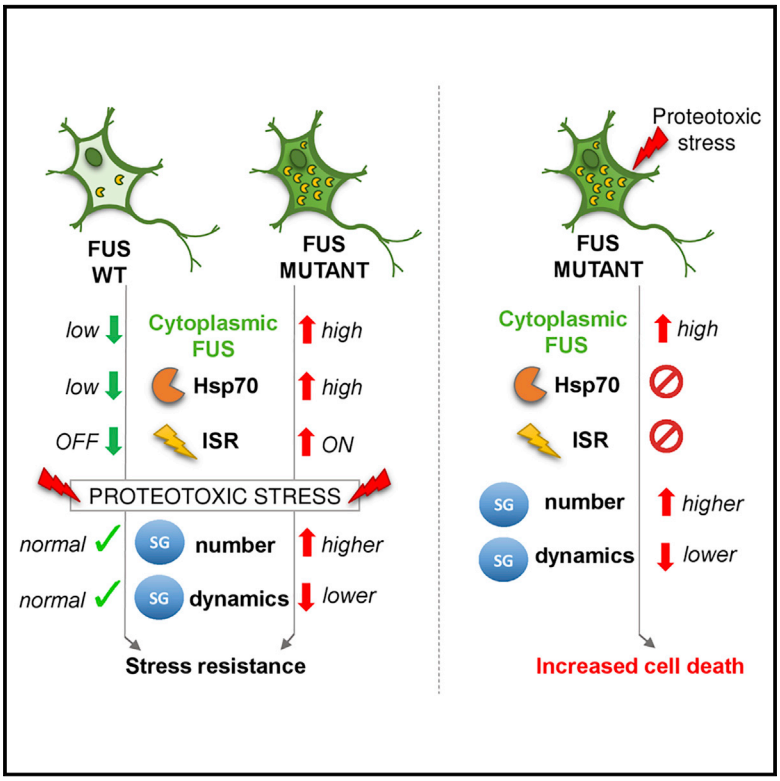

Highlights

- FUS ALS motor neurons show early activation of major stress response pathways
- Blocking SG formation does not influence survival of neurons early in FUS ALS
- Proteotoxicity is the main driver of cell death in the early stages of FUS ALS
- Stress pathways preventing proteotoxicity are a rescue mechanism in early FUS ALS

Authors

Barbara Szewczyk, René Günther, Julia Japtok, Moritz J. Frech, Marcel Naumann, Hyun O. Lee, Andreas Hermann

Correspondence

andreas.hermann@med.uni-rostock.de

In brief

Szewczyk et al. show that, in FUS ALS motor neurons, major stress response pathways are activated early, preventing proteotoxicity-driven cell death. Blocking integrated stress responses early in FUS ALS might not be beneficial. Similarly, preventing early stress granule formation is not protective in spite of signs of their aberrant dynamics.

Szewczyk et al., 2023, Cell Reports *42*, 112025
February 28, 2023
https://doi.org/10.1016/j.celrep.2023.112025

Cell Reports

CellPress
OPEN ACCESS

Article

FUS ALS neurons activate major stress pathways and reduce translation as an early protective mechanism against neurodegeneration

Barbara Szewczyk,[1] René Günther,[2,3] Julia Japtok,[2] Moritz J. Frech,[1] Marcel Naumann,[1] Hyun O. Lee,[4] and Andreas Hermann[1,5,6,7,*]

[1]Translational Neurodegeneration Section "Albrecht Kossel", Department of Neurology, University Medical Center Rostock, University of Rostock, Rostock, Germany
[2]Department of Neurology, Technische Universität Dresden, Dresden, Germany
[3]Deutsches Zentrum für Neurodegenerative Erkrankungen (DZNE) Dresden, Dresden, Germany
[4]Department of Biochemistry, Faculty of Medicine, University of Toronto, Toronto, ON, Canada
[5]Deutsches Zentrum für Neurodegenerative Erkrankungen (DZNE) Rostock/Greifswald, Rostock, Germany
[6]Center for Transdisciplinary Neurosciences Rostock (CTNR), University Medical Center Rostock, University of Rostock, Rostock, Germany
[7]Lead contact
*Correspondence: andreas.hermann@med.uni-rostock.de
https://doi.org/10.1016/j.celrep.2023.112025

SUMMARY

Amyotrophic lateral sclerosis (ALS) is a neurodegenerative disorder causing progressive loss of motor neurons. Mutations in *Fused in sarcoma* (*FUS*) leading to its cytoplasmic mislocalization cause a subset of ALS. Under stress, mutant FUS localizes to stress granules (SGs)—cytoplasmic condensates composed of RNA and various proteins. Aberrant dynamics of SGs is linked to the pathology of ALS. Here, using motor neurons (MNs) derived from human induced pluripotent stem cells, we show that, in mutant FUS, MN dynamics of SGs is disturbed. Additionally, heat-shock response (HSR) and integrated stress response (ISR) involved in the regulation of SGs are upregulated in mutant MNs. HSR activation correlates with the amount of cytoplasmic FUS mislocalization. While inhibition of SG formation, translation, or ISR does not influence survival of FUS ALS neurons, proteotoxicity that cannot be compensated with the activation of stress pathways is the main driver of neurodegeneration in early FUS ALS.

INTRODUCTION

Amyotrophic lateral sclerosis (ALS) is an incurable neurodegenerative disease leading to loss of motor neurons (MNs), paralysis, and eventually death.[1] About 90% of ALS cases are sporadic (sALS) with unknown etiology, while the remaining 10% are classified as familial (fALS). Both forms are associated with mutations in more than 20 different genes,[2] including *Fused in sarcoma* (*FUS*), which accounts for up to 5% of fALS and 1% of sALS.[2,3]

FUS is an RNA- and DNA-binding protein mostly localized in the nucleus but is capable of nucleocytoplasmic shuttling.[4] It plays a role in DNA damage repair[5] and RNA metabolism.[6–8] The nuclear import of FUS is facilitated via the C-terminal nuclear localization signal (NLS).[9] Most of the ALS-causing FUS mutations are localized in this region, causing dysfunction of nuclear import and cytoplasmic mislocalization.[10–12] This leads to the formation of pathological FUS aggregates that are enriched, among others, in the components of stress granules (SGs).[13]

SG are membraneless compartments containing mostly mRNA stalled in translation initiation or prematurely released from the polysome and multiple proteins. The assembly of SGs is a transient cellular response to stress, causing repression of global protein translation and increase in translation of stress-related transcripts.[14] Multiple reports showed that while localized to the cytoplasm, mutant FUS is recruited to SG and affects their dynamics, causing formation of larger and more abundant SGs.[15–17] The presence of these altered SGs was suggested to correlate with increased cell death.[17]

Aggregation of FUS and regulation of SG dynamics are linked to protein quality control (PQC) machinery,[18,19] and imbalance in protein homeostasis (proteostasis) is considered to be a significant factor in the development of ALS. Due to the presence of protein aggregates in degenerating neurons, the involvement of heat-shock proteins (HSPs) in the disease is of particular interest. HSPs are molecular chaperones guarding proper conformation and folding of proteins and preventing aggregation.[20] HSPs are expressed constitutively but are further induced in response to various stresses through the stress pathway called heat-shock response (HSR).[21] However, PQC capacity and HSP levels decline during aging and in neurodegenerative disorders.[22] The role of HSPs in ALS has been previously studied particularly in case of SOD1 ALS[23–28] and TDP-43 ALS,[29] and it was shown that HSPs can reduce protein aggregation and enhance survival. Additionally, main types of HSPs such as Hsp70 and its co-chaperones were shown to regulate SG

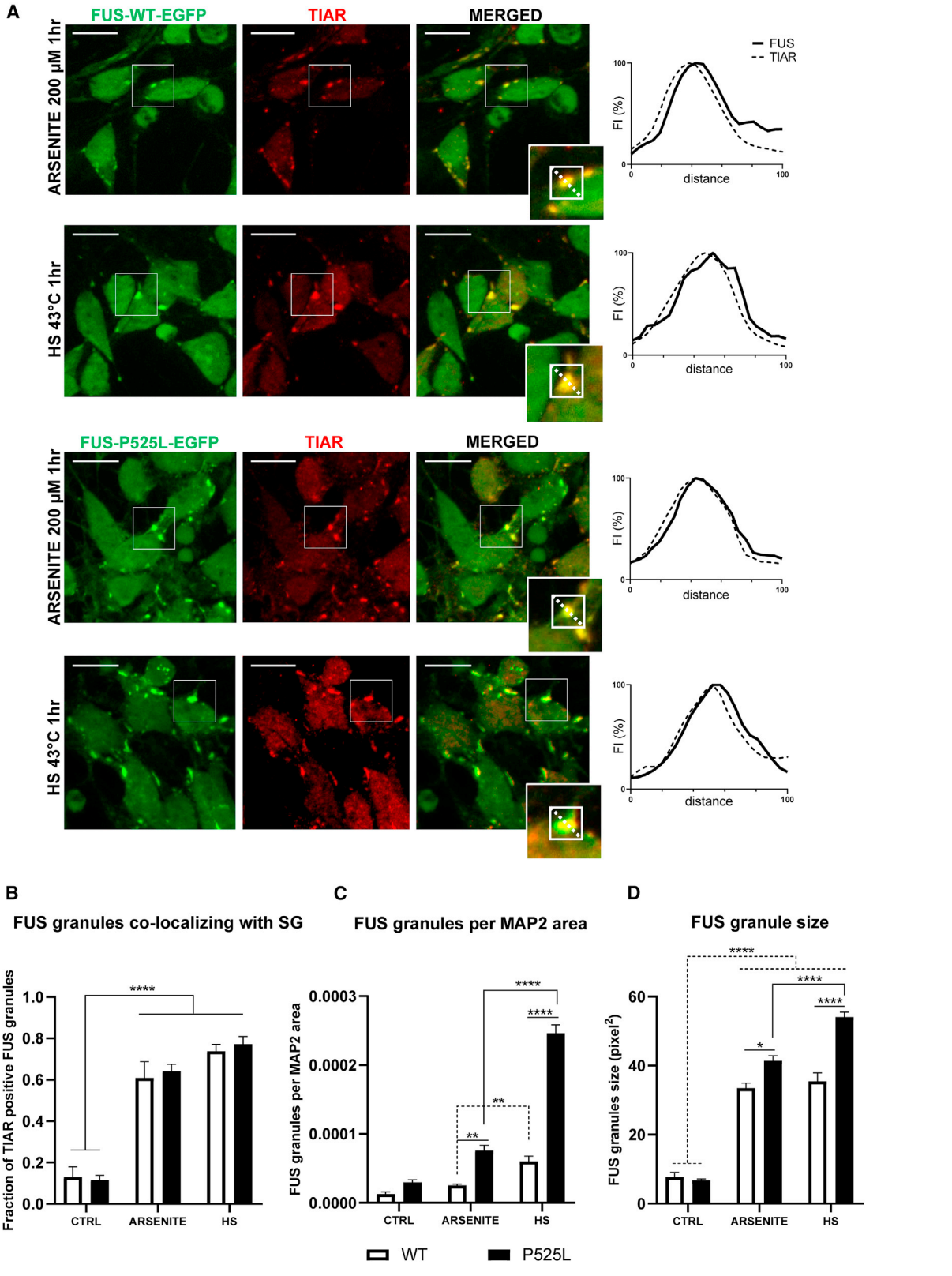

(legend on next page)

dynamics, clearance, and proper composition.[30–32] However, the involvement of HSPs in FUS ALS, particularly in human MNs, in the context of SG dynamics and at early stages of FUS ALS pathology has not yet been explored.

Another major stress pathway regulating SG formation involved in the pathology of ALS is integrated stress response (ISR).[33] ISR signals through four protein kinases activated by different stressors. For instance, endoplasmic reticulum (ER) stress activates PERK kinase, causing reduced global protein translation by phosphorylation of eukaryotic translation initiation factor 2 (eIF2α), formation of SGs, and selective expression of stress response genes.[34,35] The main effector of PERK-mediated ISR is the transcription factor Atf4 that orchestrates stress response and cell survival.[36] ISR is proposed to play a crucial role in different neurodegenerative diseases.[33] In the case of FUS ALS, it was shown that, when human mutant FUS is expressed in murine MN, it activates ISR, causing local suppression of protein translation in the axon.[37] However, the exact role of ISR in FUS ALS pathology and its potential as a therapeutic target remain unclear.

Here, we demonstrate that MNs derived from human induced pluripotent stem cells (hiPSCs) carrying ALS causing P525L FUS mutation within the NLS showed disturbed dynamics of SGs. Proteins involved in HSR and in regulation of SGs, in particular Hsp70, were upregulated in P525L FUS MNs. Inhibition of Hsp70 led to dramatic delay of SG disassembly, particularly in P525L FUS cells. Additionally, ISR was activated in P525L FUS neurons and this was associated with decreased translation rates. Despite basal activation of the stress response pathways, reduced translation, and excessive formation of SG, P525L FUS neurons did not show increased cell death in either the basal condition or upon stress. However, upon proteotoxic stress combined with translation inhibition that disabled further activation of stress response pathways, P525L neurons were more vulnerable to cell death compared with wild-type (WT). In summary, we identified ISR and HSR as early protective mechanisms that prevent P525L FUS neurons from death upon proteotoxic overload, while SG pathway inhibition, HSR inhibition, or ISR inhibition did not influence survival.

RESULTS

P525L FUS interacts with and affects SGs

To analyze the role of FUS mutation in the dynamics of SGs in human MNs, we used previously generated isogenic hiPSCs in which WT or P525L FUS protein is expressed on the endogenous level and carries an EGFP tag introduced using CRISPR-Cas9. We differentiated the cells into MNs as described previously.[38] To induce the formation of SGs, we treated MNs with either sodium arsenite or heat stress (HS). We then immunostained the neurons using TIAR as a marker of SGs (Figure 1A) and MAP2 as a marker of neurons (Figure S1A). Both WT and P525L FUS MNs showed formation of cytoplasmic FUS granules upon stress, and most of these granules co-localized with SG marker (Figures 1A and 1B). Interestingly, in the non-stressed conditions, we also detected small cytoplasmic FUS puncta negative for an SG marker in both WT and P525L FUS neurons, although they were more abundant in mutant cells (Figures S1B and S1C). Using DCP1a as a marker, we also analyzed co-localization of FUS with P-bodies, which are another type of RNA processing membraneless compartments. However, most of the FUS granules did not co-localized with P-bodies (Figures S1D–S1F). Overall, P525L FUS neurons showed significantly more abundant and larger FUS-positive SGs compared with WT in response to all the conditions, but it was the most pronounced in the case of HS (Figures 1C and 1D).

P525L FUS mutation alters the dynamics of SGs in MNs

Liquid-like properties of SG regulate their size and number.[14,39] Because we observed differences in the latter in P525L FUS neurons, we wanted to assess if liquid-like dynamics of the granules is affected by the FUS mutation. We stressed the cells as done previously, and using FUS-EGFP as a marker, we photobleached single SGs to measure the half-time recovery of the EGFP fluorescence (fluorescence recovery after photo bleaching [FRAP]; Figure 2A). P525L FUS SGs induced with arsenite, but not with HS, showed significantly increased half-time recovery compared with WT SGs (Figures 2B and 2C), which did not correlate with the size of the granules (Figure S1G).

We next focused on the SGs induced with arsenite treatment to evaluate if the difference in half-time recovery between WT and P525L FUS granules alters their disassembly. We stressed the neurons with arsenite and let them recover, analyzing the FUS-EGFP SG number over time. Initially, P525L FUS neurons showed a significantly increased SG number compared with WT, but after 120 min of recovery, both WT and P525L FUS neurons reduced the number of granules back to the basic level (Figure 2D). Next, we wanted to assess the disassembly rates of HS-induced SGs. We heat stressed the cells and quantified the SG number over recovery time as done previously. Interestingly, the disassembly of SGs induced with HS was slower in WT and P525L MNs compared with the recovery after arsenite, and this effect was more pronounced in mutant cells (Figure 2E).

HSPs are upregulated in P525L FUS MNs

HSPs are involved in the regulation of SG dynamics, including their disassembly.[32,40,41] Considering that HS is the most potent inducer of SGs and that it impairs disassembly of SGs specifically in P525L MNs, we aimed to check if this is associated with an altered expression of HSPs. We analyzed the protein level of heat-shock factor 1 (HSF1), which is a master regulator of HSR. Upon HS, HSF1 is phosphorylated and translocated to

Figure 1. FUS granules co-localizing with SG are increased in number and size in P525L FUS neurons

(A) Representative images of immunofluorescence staining of WT and P525L FUS hiPSC-MNs with an SG marker (TIAR) after respective stress; scale bar, 10 μm. The graphs show fluorescence intensity profiles of a section of a representative granule.

(B–D) Quantification of (A). FUS granules co-localizing with SG (B), FUS granule numbers (C), and FUS granule sizes (D). See also Figure S1. Data are presented as mean ± SEM. n = 3 biological replicates; for each condition, 15–30 images were analyzed. Statistical analysis with two-way ANOVA followed by Tukey's multiple comparison. *p $\leq$ 0.05; **p $\leq$ 0.01; ***p $\leq$ 0.001; ****p $\leq$ 0.0001.

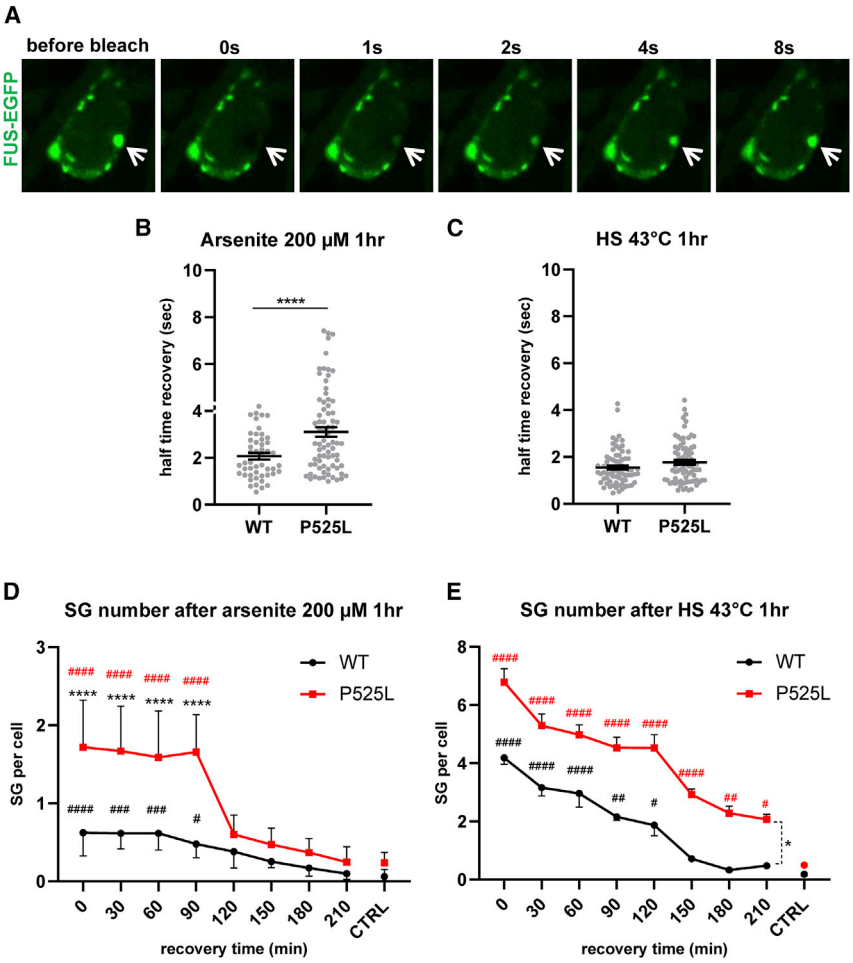

Figure 2. FUS P525L mutation alters the dynamics of FUS granules in neurons

(A) Representative time series images of a fluorescence recovery after photobleaching (FRAP) experiment. The arrow indicates a FUS-EGFP SG that was photobleached.

(B and C) Quantification of FRAP of SG induced with arsenite (A) and HS (D) represented as half-time recovery in seconds. Each point on the graph represents a single granule. Data are presented as mean ± SEM. n = 3 biological replicates; for each condition, 49–77 granules were analyzed. Statistical analysis with unpaired two-tailed Student's t test. For the samples with unequal variances, Welch's correction was applied. See also Figure S1.

(D and E) FUS granules disassembly assay after arsenite (D) or HS (E). SGs were quantified every 30 min of recovery (starting immediately after the stress withdrawal [time point 0]). The graph represents mean number of SG per cell. The asterisks indicate comparison of WT and P525L; the number signs indicate comparison of a given time point with a respective untreated control. Data are presented as mean ± SD. Some error bars are not visible due to size. n = 3 biological replicates; for each condition, 10–20 images were analyzed. Statistical analysis with two-way ANOVA followed by Tukey's multiple comparison.

*/# $p \leq 0.05$; **/## $p \leq 0.01$; ***/### $p \leq 0.001$; ****/#### $p \leq 0.0001$.

the nucleus, where it regulates the transcription of its target genes.[42] We also analyzed the level of HSF2—another member of the HSF family[43]—and a panel of major HSPs in control conditions and after HS (Figure 3A). Major chaperones—constitutively expressed Hsc70 and stress-induced Hsp70 (HspA1A, HspA1B), Hsp90 (Hsp90AA, Hsp90AB), Hsp40 (DnajB1)—and both HSF1 and HSF2 showed significantly increased levels in P525L neurons compared with WT already in non-stressed conditions (Figure 3B). Moreover, HDAC6, which regulates major pathways in response to the accumulation of protein aggregates,[44,45] was also upregulated in P525L FUS neurons (Figure 3B). While there was no significant increase in the level of any of the tested HSP directly after HS, in spite of robust phosphorylation of HSF1 (Figures 3C and S2A–S2C), we observed a significantly increased level of Hsp70 after 4 h of HS recovery in P525L neurons and after 8 h in both but a significantly higher level in mutant compared with WT cells (Figures 3D and 3E). The Hsp40 level was significantly increased after 4 h of recovery in both WT and P525L neurons (Figures 3D and 3F). The major HSPs were also upregulated in P525L FUS neuronal progenitor cells (NPCs), which are an intermediate step in our MN differentiation protocol, indicating that HSR activation is an early event in FUS ALS (Figures S2D and S2E). We also tested activation of HSR in MNs after arsenite stress. Although we detected phosphorylation of HSF1, and there was a trend showing increased HSP level in both cell lines, the HSR activation was lower compared with the HS (Figures S2F–S2H). Overall, these data led us to hypothesize that FUS mislocalization may influence proteostasis and thereby lead to an activation of the chaperone system, affecting the dynamics of SG and, more generally, stress response.

Severe FUS cytoplasmic mislocalization and FUS overexpression can activate HSR

We thus wanted to assess if other known ALS-causing FUS mutations are associated with activation of HSR. We included in the analysis two additional hiPSC lines carrying FUS NLS point mutations (R521L and R521C), one FUS NLS truncation mutation (R495QfsX527), and two healthy control lines (Table S1), and we analyzed the protein level of HSF1 and Hsp70 in hiPSC-derived MNs as done previously. Surprisingly, although there was no difference in the HSF1 level between the controls and FUS mutant MNs (Figures 4A and S3A), the Hsp70 level was significantly affected (Figures 4B and S3B). In the R521L and R521C neurons, which are considered to be associated with lower FUS cytosolic mislocalization and milder disease course,[12,46] the Hsp70 protein level was decreased compared with controls. Meanwhile, in the case of the R495QfsX527 mutation that, similarly to the P525L mutation, leads to severe cytoplasmic accumulation of FUS and more aggressive disease course,[12,46] the Hsp70 level was significantly increased. We then quantified the FUS nuclear-to-cytosolic (N/C) ratio in the

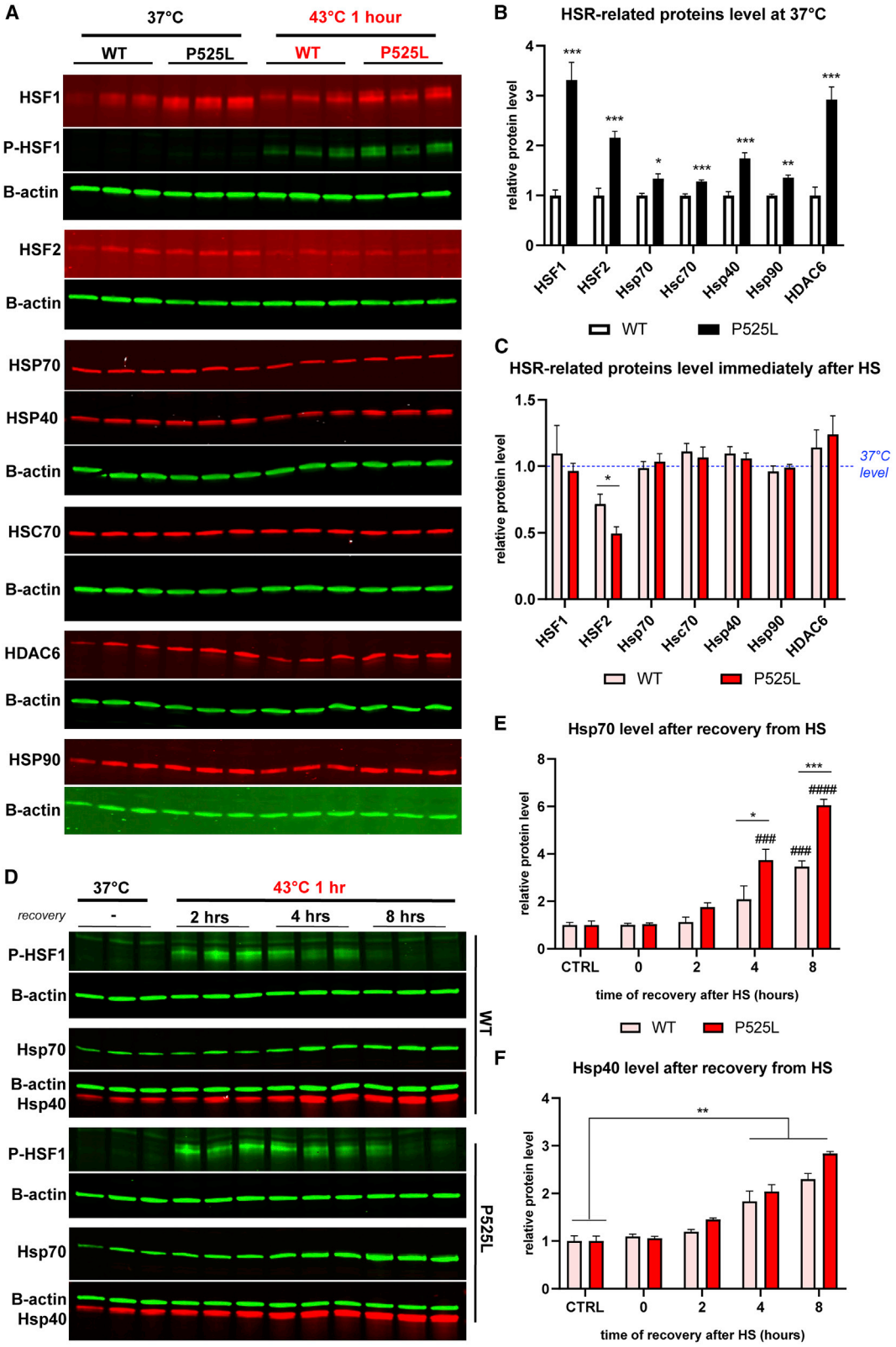

(legend on next page)

disease cell lines (Figures 4C, S3C, and S3D), and we analyzed the correlation between cytosolic FUS levels and Hsp70 levels (Figure 4D). We found a strong positive correlation between cytoplasmic FUS mislocalization and Hsp70 levels in disease condition (Figure 4D), indicating that severe accumulation of FUS in the cytoplasm leads to the activation of HSR, while milder mislocalization might be associated with a different pathological mechanism. Next, we asked whether overexpression of WT FUS, which was previously shown to mimic FUS ALS-associated neurodegeneration,[47] could also activate HSR. We used HEK293 cells with a doxycycline-inducible expression of WT FUS. We treated the cells with doxycycline for up to 48 h, and we observed a significant increase of the FUS WT protein level after that time (Figure 4E), which was also accompanied by an increase of cytoplasmic FUS (Figures S3E and S3F). This was also associated with a significant upregulation of HSF1 (Figures 4G and 4H). This suggests that increased levels of cytoplasmic FUS caused by either NLS mutation or FUS overexpression trigger FUS-mediated activation of HSR.

P525L FUS neurons rely on Hsp70 to manage excessive formation and disassembly of SGs

It was previously shown that Hsp70 promotes proper SG disassembly.[41] Therefore, we hypothesized that increased levels of Hsp70 in P525L neurons might aid the cells to properly disassemble SGs after arsenite stress (Figure 2D), whereas after HS, the chaperone network might be overwhelmed due to severe global protein aggregation, leading to delayed SG disassembly (Figure 2E). In line with this, HS caused stronger activation of HSR than arsenite, suggesting a higher demand for chaperones after HS (Figures 3D–3F and S2F–S2H). To address this further, we analyzed the level of protein aggregation after arsenite treatment and after HS using the filter retardation assay, and we observed a significant increase in protein aggregation after HS but not after arsenite treatment (Figures S4A and S4B), indicating that HS leads to the overload of chaperone network, making it unavailable for proper SG disassembly. Considering this, we next analyzed the role of Hsp70 in the disassembly of arsenite-induced SG. We stressed the neurons with arsenite in the presence or absence of the ATP-competitive Hsp70 inhibitor (Hsp70i) VER-155008,[48] and we quantified SGs over the recovery time that included continuous treatment with Hsp70i. We observed that Hsp70i caused a complete inhibition of SG disassembly or even increased levels of SG over time, which was much more pronounced in the P525L neurons (Figures 5A and 5B), while assembly of SG was not affected (Figures S4C and S4D). P525L FUS SGs showed also a significant increase in size over time compared with WT (Figures S4E–S4G). We then exposed the neurons to HS in the absence or presence of Hsp70i, and we analyzed the dynamics of SGs using FRAP. There was a significant increase of the half-time recovery for P525L FUS when HS was combined with Hsp70i (Figure 5C), indicating that Hsp70 also regulates SG liquid-like properties. Interestingly, treatment with Hsp70i alone did not induce SG formation (Figure S5A). However, when Hsp70i was combined with a potent SG inducer, puromycin,[49] neurons showed a robust formation of SG (Figures S5B–S5E), suggesting that Hsp70 is not a key factor in the process of SG formation.

P525L FUS activates ISR in human MNs

Since it was previously reported that ER stress, which is an activator of the PERK-Atf4 ISR axis,[50] is increased in ALS[51] and that ISR is activated in FUS ALS mouse model,[37] we next wanted to test whether ISR is also activated in human P525L FUS neurons. We analyzed Atf4 protein levels in WT and P525L neurons and showed that the Atf4 protein level was significantly elevated in P525L cells compared with WT (Figures 5D and 5E), implicating activation of ISR. Treatment with a known ISR inhibitor (ISRIB)[52] for 24 h led to a significant decrease of the Atf4 protein level in mutant cells, although it was still elevated compared with WT (Figures 5D and 5E). To test whether ISR activation leads to reduced translation in mutant cells, we analyzed the level of FUS protein after the treatment with ISRIB. Interestingly, western blot revealed that in P525L neurons, which are heterozygotes carrying an endogenous *WT FUS* allele and CRISPR-generated EGFP-tagged *P525L FUS* allele, the cells did not express WT FUS protein, which was in contrast to WT FUS cells that expressed both endogenous and EGFP-tagged FUS (Figure 5F). The genotype of the cell lines was carefully analyzed with PCR and sequencing (Naumann et al.[38]; Figures S5F–S5H), and this confirmed that both cell lines are heterozygotes, suggesting that P525L FUS expression led to suppression of WT FUS. The analysis revealed also that the P525L FUS protein level is higher compared with WT and that it increases further upon ISRIB treatment (Figures 5F and 5G). This indicates that activation of ISR might be a protective mechanism counteracting pathological overexpression of mutant FUS and, more generally, reducing translation to compensate for disturbed proteostasis by relieving the production of faulty protein species. We also analyzed the protein level of Hsp70 and Hsp40 after ISRIB treatment, and we did not observe any effect

Figure 3. HSPs are upregulated in P525L FUS motor neurons

(A) Representative images of fluorescent western blot for chosen HSPs in WT and P525L FUS neurons in control conditions and after 1 h of HS.

(B and C) Quantification of (A). (B) Level of the proteins in control conditions (37°C). The data were normalized to β-actin and to WT. (C) Level of proteins after HS compared with control conditions. The data were normalized to β-actin and to the level of the same protein in the control conditions. The plots represent mean ± SEM. n = 3 biological replicates. Statistical analysis with unpaired Student's t test, comparing samples from WT and P525L FUS neurons for each protein independently.

(D) Representative images of fluorescent western blot for chosen HSPs in WT and P525L FUS neurons in control conditions and after 1 h of HS followed by up to 8 h of recovery at 37°C. The asterisks indicate comparison of WT and P525L; the number signs indicate comparison with untreated control.

(E and F) Quantification of (D). The data were normalized to β-actin and to the respective non-heat-stressed control. The asterisks indicate comparison of WT and P525L; the number signs indicate comparison with untreated control. The plots represent mean ± SEM. n = 3 biological replicates. Statistical analysis with two-way ANOVA followed by Tukey's multiple comparison.

*/# $p \leq 0.05$; **/## $p \leq 0.01$; ***/### $p \leq 0.001$; ****/#### $p \leq 0.0001$

See also Figure S2.

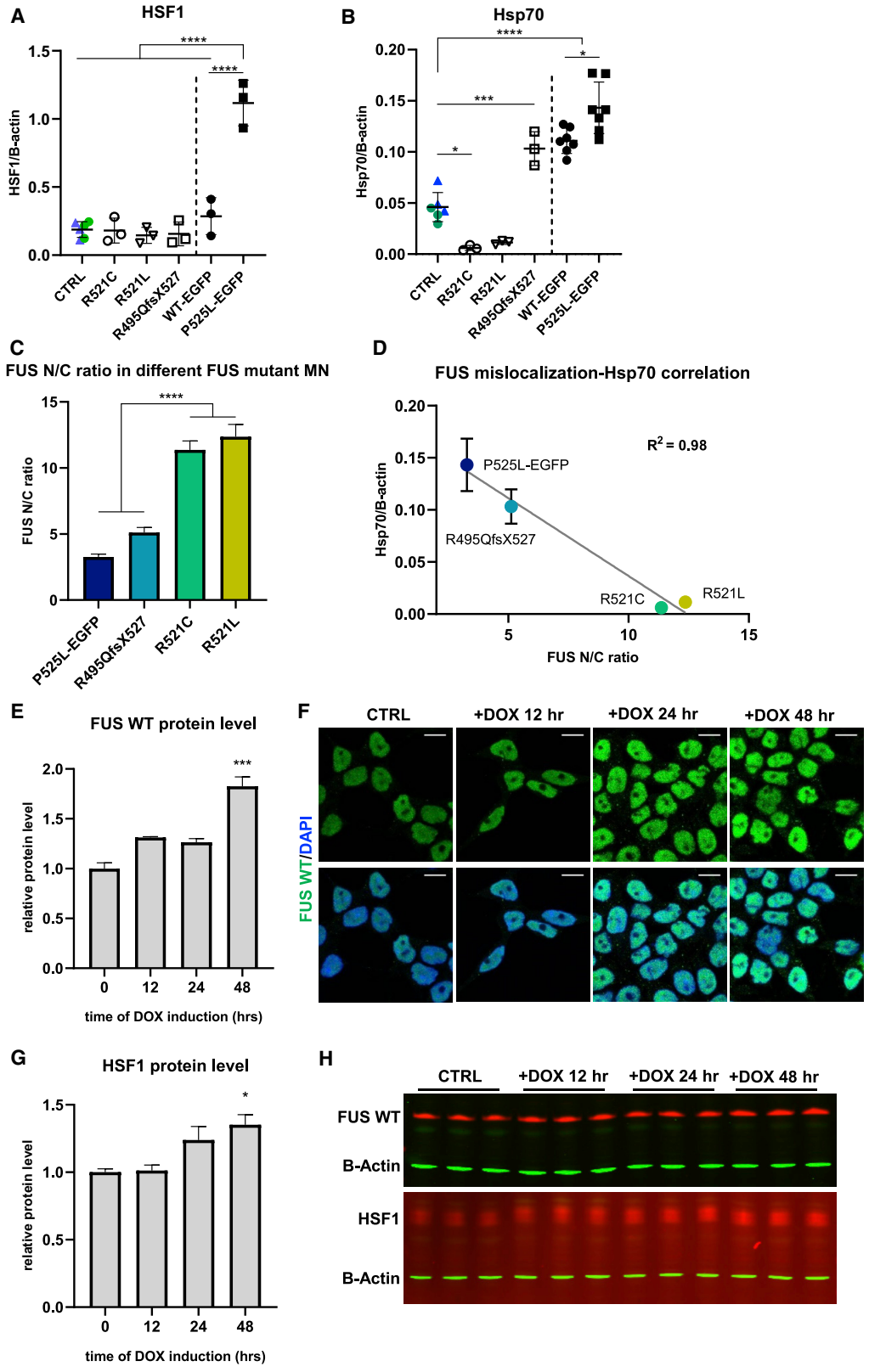

(legend on next page)

(Figures 5H–5J). This suggests that ISR and HSR activation in response to FUS mutation are, to some extent, independent from each other.

Inhibition of ISR and SG formation does not affect neuron survival upon prolonged stress

It was previously reported that ISR activation in the FUS ALS mouse model suppresses local translation in the axon, which leads to neurodegeneration.[37] Therefore, we wanted to assess if ISR inhibition with ISRIB might be beneficial for survival of mutant MNs exposed to additional stress exerted by arsenite. ISRIB functions downstream of eIF2α phosphorylation[53] (Figure 6A), and it can only inhibit ISR during mild stress, when the level of phosphorylated eIF2α does not surpass a critical level.[54] To induce mild stress, we treated the cells with low-dose arsenite, and we found that in these conditions, ISRIB blocks ISR, as indicated by inhibition of SG formation (Figures S6A and S6B). Next, we assessed viability of the neurons after 48 h of treatment. Interestingly, we did not observe any differences in the cell viability between WT and mutant neurons either in the control conditions or after arsenite and ISRIB treatment (Figure 6B). This indicates that ISR and formation of SGs are not the main pathways involved in the cell survival/cell death of mutant FUS MNs early in the pathology. We next wanted to investigate if exposure to acute stress can reveal differences in survival between WT and P525L FUS MNs. For this reason, we exposed the cells to acute arsenite stress or HS, and we analyzed their viability directly after the exposure or after 24 h recovery. However, we did not observe any decline in viability directly after the arsenite or HS exposure (Figures 6C and 6D). After 24 h of recovery, there was a significant decline of viability in cells exposed to HS but not arsenite, although there was no difference between WT and P525L neurons (Figures 6C and 6D). While both arsenite and HS are strong activators of ISR[55,56] and HSR in neurons (Figures 3D–3F and S2F–S2H), HS exerts a more proteotoxic effect on the cell (Figures S4A and S4B), which might explain its more detrimental effect. However, even in the case of highly proteotoxic stress, activation of ISR and HSR present already on the basic level and further upregulated due to stress protects mutant MNs from increased cell death.

P525L FUS neurons are at higher risk of cell death during proteotoxic stress when ISR and HSR are disabled

Considering activation of ISR in P525L neurons, which is associated with translation inhibition that was previously reported to cause neurodegeneration,[37] we next wanted to assess the role of reduced translation in the pathology of FUS ALS independently of the ISR. We used two translation inhibitors with different modes of action: cycloheximide (CHX) and puromycin.[49] Both compounds inhibit translation independently of ISR and the PERKp-eIF2α pathway[49,57] (Figure 7A). CHX blocks translation by stalling the polysome on mRNA, inhibiting polysome disassembly and blocking SG formation.[58] On the other hand, puromycin incorporates into the translated polypeptide chain, inducing disassembly of polysome, formation of SGs,[49] and release of defective ribosomal products (DRiPs), which are truncated polypeptides prone to misfolding.[59] While both compounds disable production of stress response proteins by inhibiting total translation, CHX does not show a proteotoxic effect, while puromycin does.[60] We treated neurons with either CHX or puromycin for up to 48 h, and as expected, we observed SG formation after puromycin, but not after CHX, treatment (Figure S6C). To evaluate if translation inhibition was effective, we analyzed the level of an autophagosome cargo protein p62 after the treatments. We observed a significant reduction in p62 level after 24 h of CHX treatment (Figures 7B and 7C). After puromycin treatment, we detected additional bands of smaller molecular weight and smearing on the western blot (Figure 7B), indicating the presence of truncated p62 polypeptide chains that are released prematurely from the polysome. Interestingly, we did not observe a decreased FUS protein level even after 48 h of treatment with either CHX or puromycin (Figures 7D and 7E), suggesting that FUS protein turnover is relatively slow in neurons. Next, we analyzed the cell number to assess if cell death is affected by translation inhibition. We did not observe any cytotoxic effect of CHX after 48 h of treatment (Figure 7F). In the case of highly proteotoxic puromycin, there was a significant reduction in the number of P525L FUS neurons after 48 h (Figure 7F). This suggests that reduced translation per se is not the main driver of neurodegeneration in early FUS ALS. It is rather high proteotoxicity combined with the inability to activate stress response pathways. Nevertheless, the observed effect was mild,

Figure 4. Severe FUS cytoplasmic mislocalization and FUS overexpression can activate HSR

(A and B) Relative protein level of HSF1 (A) and Hsp70 (B) in MNs derived from control and FUS ALS hiPSC lines normalized to β-actin. Representative western blot images are presented in Figure S3A. Each point on the plot represents a biological replicate (an independent differentiation, n = 3) for each cell line. Two control cell lines were pooled together. Mean ± SD is presented. Statistical analysis with one-way ANOVA followed by Tukey's multiple comparison.

(C) Quantification of nuclear-to-cytosolic (N/C) FUS ratio. MNs were immunostained with FUS antibody, and fluorescence intensity in N and C was measured. The N/C ratio of at least 23 cells was calculated after applying background correction. The plot represents mean ± SEM. Statistical analysis with one-way ANOVA followed by Tukey's multiple comparison.

(D) Linear regression analysis of the correlation between FUS N/C ratio shown in (C) and Hsp70 level shown in (B).

(E) Analysis of FUS WT level in HEK293 cell with doxycycline-inducible expression of FUS WT after up to 48 h of doxycycline treatment. The plot represents quantification of FUS WT protein level based on the fluorescent western blot (shown in H) and shows mean ± SEM. n = 3 samples from independent experiments. Statistical analysis with one-way ANOVA followed by Tukey's multiple comparison.

(F) Representative images of immunostaining of FUS in HEK293 cells with doxycycline-inducible expression of FUS WT after up to 48 h of doxycycline treatment. Scale bar, 10 μm.

(G) Quantification of HSF1 protein in doxycycline-treated FUS WT HEK293 based on the fluorescent western blot presented in (H). The plot represents mean ± SEM. n = 3 samples from independent experiments. Statistical analysis with one-way ANOVA followed by Tukey's multiple comparison.

(H) Fluorescent western blot for FUS WT and HSF1 in doxycycline-treated FUS WT HEK293 cells.

*p ≤ 0.05; **p ≤ 0.01; ***p ≤ 0.001; ****p ≤ 0.0001.

See also Figure S3.

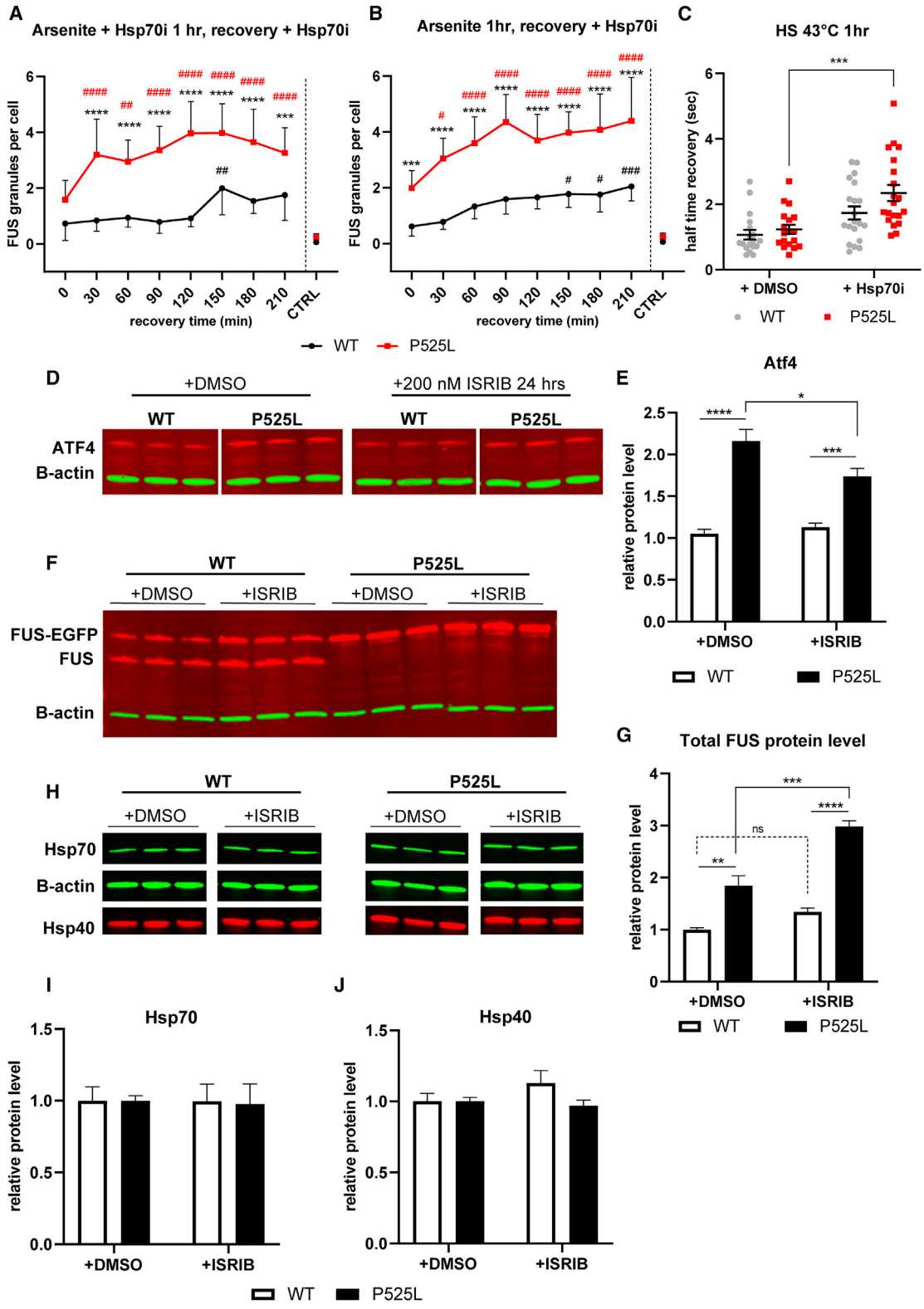

Figure 5. P525L FUS neurons rely on Hsp70 to manage excessive formation and disassembly of SG and show activation of ISR

(A and B) FUS granules disassembly assay. The neurons were stressed with arsenite and Hsp70i (A) or with arsenite alone (B) and left to recover with a continuous inhibition of Hsp70. SGs were quantified every 30 min of recovery. The graphs represent the number of SGs per cell at each time point. Data are presented as

(legend continued on next page)

as neurons showed surprising resistance to the translation inhibition. It was shown previously that in terminally differentiated neurons, global translation is lower compared with NPCs.[61] Therefore, to validate our findings, we treated WT and P525L FUS NPCs with CHX or puromycin, and we analyzed the FUS protein level. We observed a significant decrease in both WT and P525L FUS protein levels over time (Figures S6D and S6E), confirming that NPCs have higher FUS turnover. Next, we analyzed the cell death of treated NPCs. After 48 h of CHX treatment, there was a significant reduction of the cell number for both WT and P525L FUS NPCs, but there was no significant difference between WT and P525L FUS cells (Figure S6F). In contrast, puromycin treatment had a much stronger impact on the survival of P525L FUS NPCs. After 48 h of treatment, there were no more surviving P525L FUS cells, while 40% of WT FUS NPCs survived (Figure S6G).

DISCUSSION

The localization of ALS-associated mutant FUS into SGs under stress is a well-documented phenomenon.[9,16,62–64] Here, using hiPSC-derived MNs, we demonstrated that P525L FUS localizes into SGs and alters their abundance, size, and dynamics. While others described that mutant FUS may accelerate the disassembly of SGs *in vitro*[15] or delay it *in vivo*,[17] we observed a significant delay in the disassembly of HS-induced SGs in P525L FUS neurons compared with WT, which was not the case for the arsenite-induced SGs. Stress-specific, cell-type-specific, and disease-dependent composition of SGs was previously identified and described in detail.[65,66] For instance, in HeLa cells treated with either arsenite or HS, out of 52 SG-associated proteins, only 77% co-localized with SGs under both stress conditions, while the remaining 23% were stress specific.[65] Our findings revealing differences in SG dynamics in P525L neurons depending on the used condition might be the biological consequence of this composition diversity. Similarly, we observed stress-dependent differences in SG liquid-like properties using FRAP, which did not correlate with SG disassembly dynamics. This might indicate that liquid-like properties of SGs do not directly define their disassembly rates but possibly are due to their different composition and diverse interactions of WT versus P525L FUS with SG components. Overall, these findings suggest that FUS-mutation-induced changes in SG dynamics depend largely on a broader cellular context.

We demonstrated here that FUS mutation leads to an activation of HSR in human MNs and that inhibition of Hsp70 causes further disturbance in SG processing. Interestingly, activation of HSR in MNs expressing different variants of mutant FUS depended on the level of cytoplasmic FUS mislocalization. This correlated with the disease course showing earlier onset and more rapid progression in the case of mutations associated with higher levels of cytoplasmic FUS.[12] In line with this, overexpression of WT FUS and its accumulation in the cytoplasm also increased the level of HSF1, suggesting that FUS protein is inherently capable of triggering HSR when overrepresented in the cytoplasm. This toxic gain of function of FUS is currently targeted by a phase 3 clinical trial that shows promising results of antisense oligonucleotide approach to reduce overall FUS level.[67]

Many reports have analyzed the collapse of proteostasis as a potential pathological event during ALS development.[24–29] However, the impact of FUS mutation on the expression of chaperones in human neurons has not been analyzed in depth so far. We speculate that upregulation of HSPs in response to the FUS mutation reported here is an early event in ALS since hiPSC-derived neurons are comparable with the fetal developmental stage.[68] As proteostasis is compromised with aging and neurodegeneration,[69,70] it is likely that neurons lose the capability to upregulate HSP in response to FUS mutation with time, which may lead to a disrupted clearance of SG and FUS aggregation and a fatal decline of proteostasis. Increased levels of chaperones in P525L neurons might explain that in spite of formation of arsenite-induced SGs that are larger and more abundant and show altered dynamics, the disassembly process is not affected. On the contrary, the disassembly of HS-induced SGs is significantly delayed in P525L FUS neurons. We propose that during HS, the chaperone network is overwhelmed with assisting multiple aggregating clients, and thus the capacity for SG disassembly is not sufficient. Interestingly, it was also shown that SGs in MNs are particularly enriched in components of PQC proteins compared with other cell types.[65] Therefore, MNs might be particularly vulnerable to depletion of these components. In line with this, inhibition of Hsp70 leads to the stiffening of the granules and to suppression of their disassembly, which is more

mean ± SD. n = 3 biological replicates; for each condition, at least 13 images were analyzed. Statistical analysis with two-way ANOVA followed by Tukey's multiple comparison. The asterisks represent the difference between WT and P525L FUS neurons at each time point; the number signs represent the difference between a given time point and the time point zero.

(C) Quantification of FRAP of SGs induced with HS and HS combined with Hsp70i in WT and P525L neurons. Each point on the graph represents a single granule. Data are presented as mean ± SEM. n = 3 biological replicates; for each condition, 18–20 FUS granules were analyzed. Statistical analysis with two-way ANOVA followed by Tukey's multiple comparison.

(D) Fluorescent western blot for Atf4 and eIF2α in WT and P525L FUS MNs in the control condition and after treatment with ISRIB.

(E) Quantification of (A). The graph represents mean ± SEM. n = 3 biological replicates. Statistical analysis with two-way ANOVA followed by Tukey's multiple comparison.

(F) Fluorescent western blot for FUS protein in WT and P525L FUS MNs in the control condition and after treatment with ISRIB.

(G) Quantification of (F). The graph represents mean ± SEM. n = 3 biological replicates. Statistical analysis with two-way ANOVA followed by Tukey's multiple comparison.

(H) Fluorescent western blot for selected HSPs in WT and P525L FUS MNs in the control condition and after treatment with ISRIB.

(I and J) Quantification of (H). The graph represents mean ± SEM. n = 3 biological replicates. Statistical analysis with two-way ANOVA followed by Tukey's multiple comparison.

*p ≤ 0.05; **p ≤ 0.01; ***p ≤ 0.001; ****p ≤ 0.0001.

See also Figure S5.

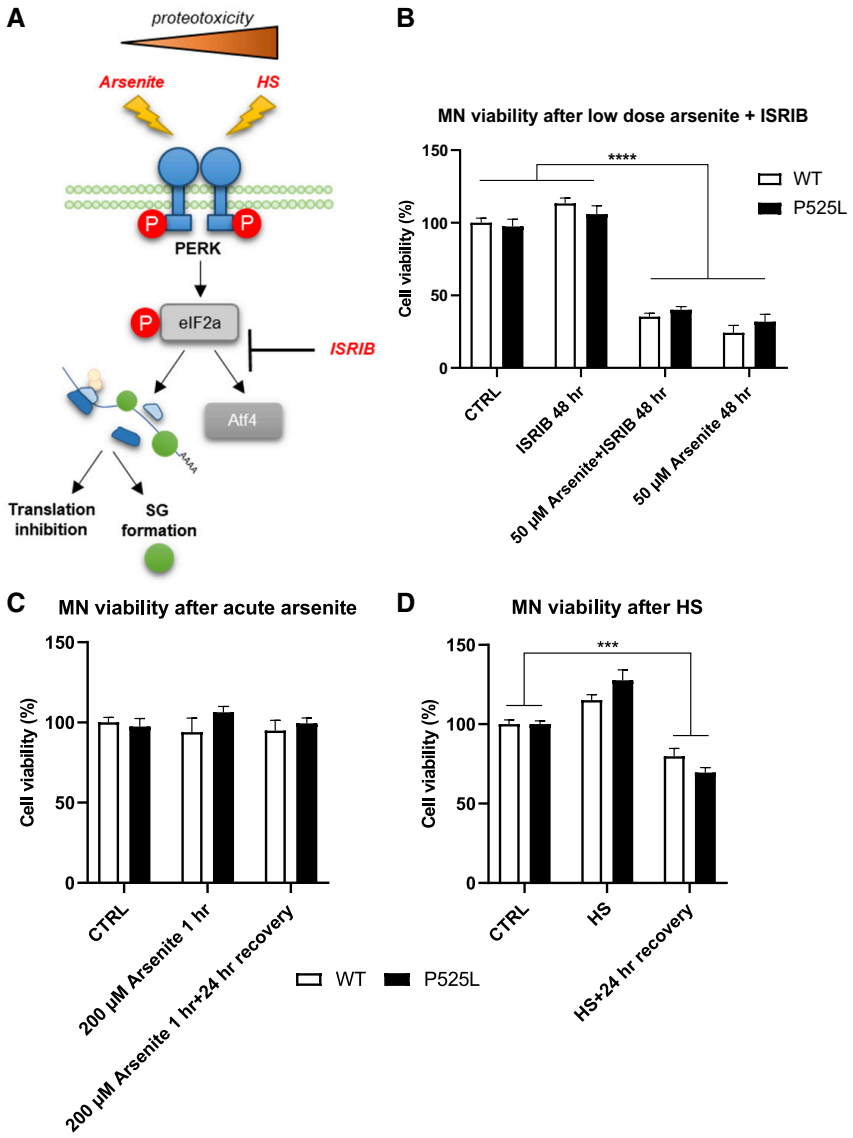

Figure 6. Proteotoxicity and SG formation do not cause increased cell death of P525L FUS neurons when the protective mechanism can be activated

(A) A schematic overview of ISR PERK-Atf4 pathway activated by HS and sodium arsenite.

(B–D) Survival assay for the cells treated with low-dose arsenite and ISRIB after 48 h (B) and with high does arsenite (C) and HS (D) after 1 and 24 h recovery, respectively. The viability was assessed with PrestoBlue assay. The graph represents the cell viability as a percent of untreated control. Data are presented as mean ± SEM. n = 3 biological replicates; for each biological replicate, there are 4 technical replicates. Statistical analysis with two-way ANOVA followed by Tukey's multiple comparison.

*p ≤ 0.05; **p ≤ 0.01; ***p ≤ 0.001; ****p ≤ 0.0001. See also Figure S4 and S6.

severe in P525L FUS neurons. It was reported previously that Hsp70 prevents formation of aberrant SGs in the presence of misfolding mutant SOD1 protein and that it is essential for SG disassembly,[41] additionally supporting the importance of this chaperone in the maintenance of proper SG functions.

We also describe here activation of the ISR in P525L FUS human MNs. Activation of ISR was previously reported in the context of neurodegenerative disorders, and also in the case of FUS ALS,[37] and it was often associated with ER stress and loss of proteostasis.[33] Although it remains unclear whether ISR is a cause or a symptom of neurodegeneration, its persistent activation in P525L FUS neurons might be involved in the excessive formation of SGs. We showed that downregulation of ISR causes an increase in FUS protein levels specifically in P525L FUS neurons, indicating that translation is already suppressed to some extent in mutant neurons and that activation of ISR reduces, albeit not completely, overexpression of FUS protein caused by the mutation, which on its own is detrimental to the neurons.[47]

We demonstrated that there is no difference in the survival between WT and P525L neurons under various stress conditions. This suggests that (over)activation of stress response pathways in the mutant cells protects them from increased susceptibility to cell death early in the disease course even under proteotoxic overload and in spite of altered SG dynamics. At the same time, inhibiting ISR during stress exposure did not change that outcome, suggesting that ISR on its own is not responsible for this protective effect. However, P525L neurons are more susceptible to cell death during prolonged translation inhibition combined with proteotoxic overload.

Our results suggest that neurons show high resistance to acute and prolonged protein translation inhibition with CHX but not with proteotoxic puromycin. This indicates that pathological activation of ISR leads to neurodegeneration, possibly not through the global protein translation suppression but rather might be associated with expression of stress-related proteins with pro-apoptotic functions that are produced downstream of ISR activation.[71] In line with this, reduced translation per se is associated with longevity since it was shown to reduce the burden on the proteostatic machinery.[72,73] In addition, in the field of neurodegeneration research, there is now more focus on the proteostasis control at the level of protein synthesis, where ribosomal quality control (RQC) machinery maintains nascent polypeptide chains still associated with ribosome. It has been shown that ribosomal stalling and release of DRiPs is associated with loss of proteostasis during neurodegeneration[74,75] and that improving RQC can rescue neurodegeneration-associated phenotypes.[76] We speculate that reduced translation rates

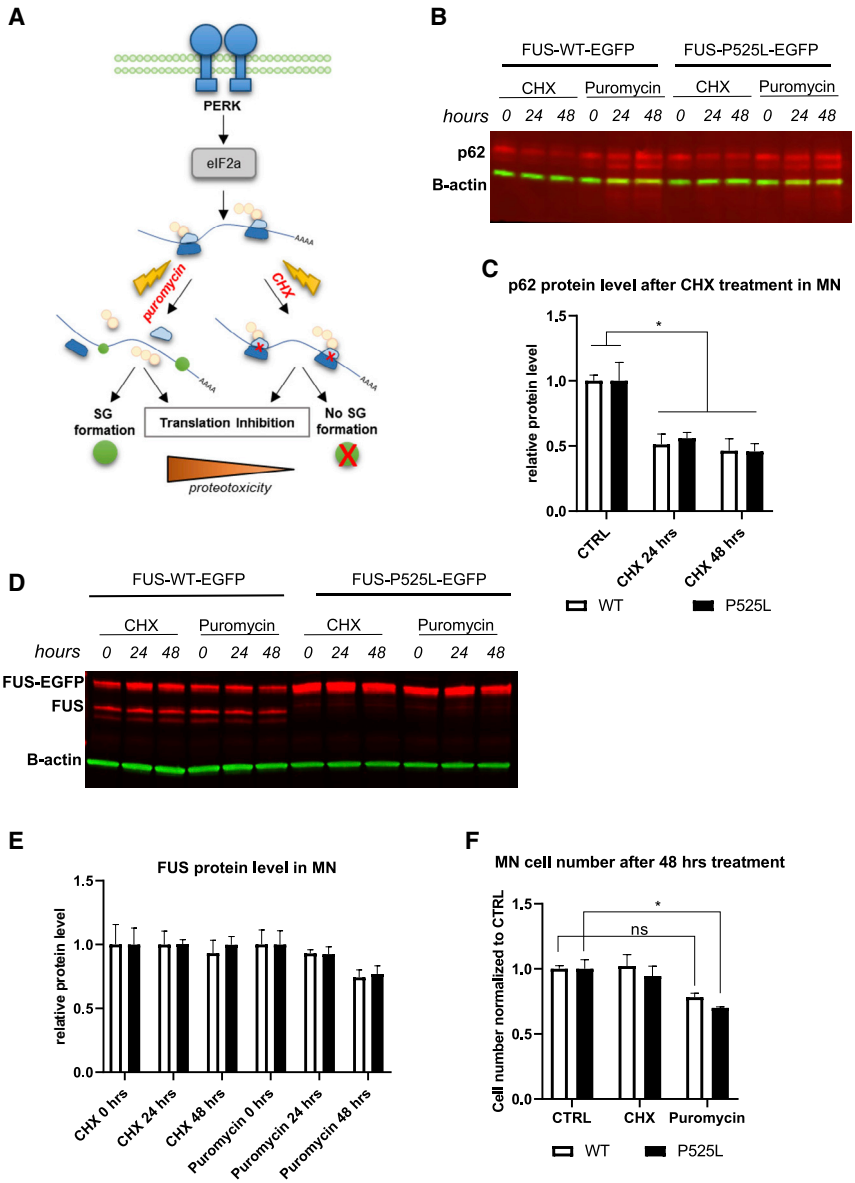

Figure 7. P525L FUS neurons show increased cell death after prolonged stress

(A) Mechanism of action of puromycin and cycloheximide.

(B) A representative image of a fluorescent western blot analysis of p62 protein level in the neurons treated with either CHX or puromycin.

(C) Quantification of (B). The graph shows level of the p62 proteins normalized to β-actin and to WT. p62 level after puromycin treatment was not quantified because of appearance of multiple bands/smearing. Data are presented as mean ± SEM. n = 3 biological replicate. Statistical analysis with two-way ANOVA followed by Tukey's multiple comparison.

(D) A representative image of a fluorescent western blot analysis of FUS protein level in the neurons treated with either CHX or puromycin for up to 48 h.

(E) Quantification of (D). The level of total FUS protein (endogenous FUS + FUS-EGFP) normalized to β-actin and to non-treated control. Data are presented as mean ± SEM. n = 3 biological replicate. Statistical analysis with two-way ANOVA followed by Tukey's multiple comparison.

(F) Quantification of the neuron cell numbers after 48 h of treatment with either CHX or puromycin. The cells were counted using the cell counter and analyzer (CASY). The cell number was normalized to untreated control. Data are presented as mean ± SEM. n = 3 biological replicates. Statistical analysis with two-way ANOVA followed by Tukey's multiple comparison.

*p ≤ 0.05; **p ≤ 0.01; ***p ≤ 0.001; ****p ≤ 0.0001; ns - not significant.

See also Figure S6.

might be one of the mechanisms that P525L neurons employ to reduce the production of DRiPs.

Interestingly, ISRIB treatment for different neurodegenerative diseases is currently discussed as it has shown some results in rescuing neurodegeneration-associated phenotypes in a mouse model of Alzheimer's disease and in a cell model of SOD1 ALS,[77,78] although some reports do not support this protective effect.[79] We speculate that the beneficial effect of ISR activation observed early in the FUS ALS pathology turns into a toxic mechanism over time; therefore, the timing and duration of a potential ISRIB treatment might be essential for observing preventive outcomes.

No effect of translation inhibition with CHX on the survival of neurons was associated with low protein turnover. Slow protein turnover in postmitotic neurons compared with cycling cells might also explain that in spite of persistent activation of ISR and decreased translation in the early stages of FUS ALS pathology, neurons remain resistant to neurodegeneration and only over an extended period do they succumb to cell death. Interestingly, we observed suppression of FUS WT expression in the presence of the P525L FUS variant in our cell model. It was previously shown that FUS autoregulates its own expression level by binding to exon7 of its mRNA, which leads to exon skipping and degradation of the transcript via nonsense-mediated decay, and that this autoregulatory mechanism is disturbed by the FUS mutation.[80] We speculate that in our model, P525L FUS escapes the autoregulatory mechanism, which leads to accumulation of the mutant protein and to downregulation of the WT variant.

In summary, we pinpointed ISR and HSR as early protective mechanisms that are activated in response to accumulation of cytoplasmic FUS in the early pathology of FUS ALS. These pathways protect P525L FUS during proteotoxic stress, which is the most harmful to the mutant neurons, and prevent their cell death. Meanwhile, aberrations in SG-related pathways and protein translation are not detrimental to neurons in the early FUS ALS.

Limitations of the study

Although using hiPSC-derived MNs gives a unique possibility to investigate patient-specific phenotypes in the disease-relevant cell type, a major shortcoming of this model for studying late-onset age-related diseases such as FUS ALS is their fetal-like developmental stage. Such neurons might carry resilience factors that *in vivo* fade over time because of aging and other environmental factors. Therefore, the magnitude of the observed effects might be moderate, and the described mechanisms might depict very early stages of the disease. Accordingly, when studying age-related disorders, it is paramount to complement studies of hiPSC-derived neurons with models that recapitulate aging hallmarks.

STAR★METHODS

Detailed methods are provided in the online version of this paper and include the following:

- KEY RESOURCES TABLE
- RESOURCE AVAILABILITY
  - Lead contact
  - Materials availability
  - Data and code availability
- EXPERIMENTAL MODEL AND SUBJECT DETAILS
- METHOD DETAILS
  - Treatments and inhibitors
  - Immunofluorescence staining and imaging
  - Quantification of FUS nuclear-to-cytosolic (N/C) ratio
  - Fluorescence recovery after photo bleaching
  - Western blot
  - Cell survival analysis
  - Filter retardation assay
- QUANTIFICATION AND STATISTICAL ANALYSIS

SUPPLEMENTAL INFORMATION

Supplemental information can be found online at https://doi.org/10.1016/j.celrep.2023.112025.

ACKNOWLEDGMENTS

We acknowledge great help in cell culture by Anett Böhme and Jette Abel. We thank Tobias M. Böckers for providing FUS R495fsX527 hiPSC and Markus Landthaler for providing FLP-293-TRex TO/FLAG-HA/FUS-WT cells. We thank Robert Haase and the Scientific Computing Facility MPI-CBG Dresden for help in the analysis of FRAP. This work was supported by the Light Microscopy Facility, a Core Facility of the CMCB Technology Platform at TU Dresden, and the Light Microscopy Facility of the MPI-CBG Dresden. This work was supported in part by the "Deutsche Gesellschaft für Muskelkranke (He2/2)" to A.H., the NOMIS Foundation to A.H., and the Helmholtz Virtual Institute "RNA dysmetabolism in ALS and FTD (VH-VI-510)" to A.H. A.H. is supported by the Hermann und Lilly Schilling-Stiftung für Medizinische Forschung im Stifterverband. R.G. was supported by "niemALS aufgeben e.V.". H.O.L. is supported by Canada Research Chairs Program and Medicine by Design initiative, which receives funding from the Canada First Research Excellence Fund.

AUTHOR CONTRIBUTIONS

Conceptualization, A.H. and B.S.; methodology, R.G., M.N., J.J., H.O.L., and M.J.F.; formal analysis, B.S. and H.O.L; investigation, B.S., R.G., and H.O.L.; resources, A.H. and J.J.; data curation, B.S.; writing—original draft preparation, B.S. and A.H.; writing—review & editing, all authors; visualization, B.S.; supervision, A.H.; project administration, A.H.; funding acquisition, A.H. All authors have read and agreed to the published version of the manuscript.

DECLARATION OF INTERESTS

The authors declare no conflict of interest.

INCLUSION AND DIVERSITY

We support inclusive, diverse, and equitable conduct of research.

Received: October 5, 2022
Revised: November 2, 2022
Accepted: January 6, 2023
Published: January 24, 2023

REFERENCES

1. Masrori, P., and Van Damme, P. (2020). Amyotrophic lateral sclerosis: a clinical review. Eur. J. Neurol. *27*, 1918–1929. https://doi.org/10.1111/ene.14393.
2. Volk, A.E., Weishaupt, J.H., Andersen, P.M., Ludolph, A.C., and Kubisch, C. (2018). Current knowledge and recent insights into the genetic basis of amyotrophic lateral sclerosis. Med. Genet. *30*, 252–258. https://doi.org/10.1007/s11825-018-0185-3.
3. Taylor, J.P., Brown, R.H., Jr., and Cleveland, D.W. (2016). Decoding ALS: from genes to mechanism. Nature *539*, 197–206. https://doi.org/10.1038/nature20413.
4. Kino, Y., Washizu, C., Aquilanti, E., Okuno, M., Kurosawa, M., Yamada, M., Doi, H., and Nukina, N. (2011). Intracellular localization and splicing regulation of FUS/TLS are variably affected by amyotrophic lateral sclerosis-linked mutations. Nucleic Acids Res. *39*, 2781–2798. https://doi.org/10.1093/nar/gkq1162.
5. Baechtold, H., Kuroda, M., Sok, J., Ron, D., Lopez, B.S., and Akhmedov, A.T. (1999). Human 75-kDa DNA-pairing protein is identical to the pro-oncoprotein TLS/FUS and is able to promote D-loop formation. J. Biol. Chem. *274*, 34337–34342. https://doi.org/10.1074/jbc.274.48.34337.
6. Yang, L., Gal, J., Chen, J., and Zhu, H. (2014). Self-assembled FUS binds active chromatin and regulates gene transcription. Proc. Natl. Acad. Sci. USA *111*, 17809–17814. https://doi.org/10.1073/pnas.1414004111.
7. Yamazaki, T., Chen, S., Yu, Y., Yan, B., Haertlein, T.C., Carrasco, M.A., Tapia, J.C., Zhai, B., Das, R., Lalancette-Hebert, M., et al. (2012). FUS-SMN protein interactions link the motor neuron diseases ALS and SMA. Cell Rep. *2*, 799–806. https://doi.org/10.1016/j.celrep.2012.08.025.
8. Belly, A., Moreau-Gachelin, F., Sadoul, R., and Goldberg, Y. (2005). Delocalization of the multifunctional RNA splicing factor TLS/FUS in hippocampal neurones: exclusion from the nucleus and accumulation in dendritic granules and spine heads. Neurosci. Lett. *379*, 152–157. https://doi.org/10.1016/j.neulet.2004.12.071.
9. Gal, J., Zhang, J., Kwinter, D.M., Zhai, J., Jia, H., Jia, J., and Zhu, H. (2011). Nuclear localization sequence of FUS and induction of stress granules by ALS mutants. Neurobiol. Aging *32*, 2323.e27–2323.e40. https://doi.org/10.1016/j.neurobiolaging.2010.06.010.
10. Kwiatkowski, T.J., Jr., Bosco, D.A., Leclerc, A.L., Tamrazian, E., Vanderburg, C.R., Russ, C., Davis, A., Gilchrist, J., Kasarskis, E.J., Munsat, T., et al. (2009). Mutations in the FUS/TLS gene on chromosome 16 cause familial amyotrophic lateral sclerosis. Science *323*, 1205–1208. https://doi.org/10.1126/science.1166066.
11. Vance, C., Rogelj, B., Hortobágyi, T., De Vos, K.J., Nishimura, A.L., Sreedharan, J., Hu, X., Smith, B., Ruddy, D., Wright, P., et al. (2009). Mutations in FUS, an RNA processing protein, cause familial amyotrophic lateral sclerosis type 6. Science *323*, 1208–1211. https://doi.org/10.1126/science.1165942.

12. Naumann, M., Peikert, K., Günther, R., van der Kooi, A.J., Aronica, E., Hübers, A., Danel, V., Corcia, P., Pan-Montojo, F., Cirak, S., et al. (2019). Phenotypes and malignancy risk of different FUS mutations in genetic amyotrophic lateral sclerosis. Ann. Clin. Transl. Neurol. *6*, 2384–2394. https://doi.org/10.1002/acn3.50930.

13. Fujita, K., Ito, H., Nakano, S., Kinoshita, Y., Wate, R., and Kusaka, H. (2008). Immunohistochemical identification of messenger RNA-related proteins in basophilic inclusions of adult-onset atypical motor neuron disease. Acta Neuropathol. *116*, 439–445. https://doi.org/10.1007/s00401-008-0415-x.

14. Protter, D.S.W., and Parker, R. (2016). Principles and properties of stress granules. Trends Cell Biol. *26*, 668–679. https://doi.org/10.1016/j.tcb.2016.05.004.

15. Baron, D.M., Kaushansky, L.J., Ward, C.L., Sama, R.R.K., Chian, R.J., Boggio, K.J., Quaresma, A.J.C., Nickerson, J.A., and Bosco, D.A. (2013). Amyotrophic lateral sclerosis-linked FUS/TLS alters stress granule assembly and dynamics. Mol. Neurodegener. *8*, 30. https://doi.org/10.1186/1750-1326-8-30.

16. Marrone, L., Poser, I., Casci, I., Japtok, J., Reinhardt, P., Janosch, A., Andree, C., Lee, H.O., Moebius, C., Koerner, E., et al. (2018). Isogenic FUS-eGFP iPSC reporter lines enable quantification of FUS stress granule pathology that is rescued by drugs inducing autophagy. Stem Cell Rep. *10*, 375–389. https://doi.org/10.1016/j.stemcr.2017.12.018.

17. Zhang, X., Wang, F., Hu, Y., Chen, R., Meng, D., Guo, L., Lv, H., Guan, J., and Jia, Y. (2020). In vivo stress granule misprocessing evidenced in a FUS knock-in ALS mouse model. Brain *143*, 1350–1367. https://doi.org/10.1093/brain/awaa076.

18. Ciechanover, A., and Kwon, Y.T. (2017). Protein quality control by molecular chaperones in neurodegeneration. Front. Neurosci. *11*, 185. https://doi.org/10.3389/fnins.2017.00185.

19. Alberti, S., Mateju, D., Mediani, L., and Carra, S. (2017). Granulostasis: protein quality control of RNP granules. Front. Mol. Neurosci. *10*, 84. https://doi.org/10.3389/fnmol.2017.00084.

20. Leak, R.K. (2014). Heat shock proteins in neurodegenerative disorders and aging. J. Cell Commun. Signal. *8*, 293–310. https://doi.org/10.1007/s12079-014-0243-9.

21. Richter, K., Haslbeck, M., and Buchner, J. (2010). The heat shock response: life on the verge of death. Mol. Cell *40*, 253–266. https://doi.org/10.1016/j.molcel.2010.10.006.

22. Labbadia, J., and Morimoto, R.I. (2015). The biology of proteostasis in aging and disease. Annu. Rev. Biochem. *84*, 435–464. https://doi.org/10.1146/annurev-biochem-060614-033955.

23. Mimoto, T., Morimoto, N., Miyazaki, K., Kurata, T., Sato, K., Ikeda, Y., and Abe, K. (2012). Expression of heat shock transcription factor 1 and its downstream target protein T-cell death associated gene 51 in the spinal cord of a mouse model of amyotrophic lateral sclerosis. Brain Res. *1488*, 123–131. https://doi.org/10.1016/j.brainres.2012.10.012.

24. Marino, M., Papa, S., Crippa, V., Nardo, G., Peviani, M., Cheroni, C., Trolese, M.C., Lauranzano, E., Bonetto, V., Poletti, A., et al. (2015). Differences in protein quality control correlate with phenotype variability in 2 mouse models of familial amyotrophic lateral sclerosis. Neurobiol. Aging *36*, 492–504. https://doi.org/10.1016/j.neurobiolaging.2014.06.026.

25. Wang, J., Xu, G., Li, H., Gonzales, V., Fromholt, D., Karch, C., Copeland, N.G., Jenkins, N.A., and Borchelt, D.R. (2005). Somatodendritic accumulation of misfolded SOD1-L126Z in motor neurons mediates degeneration: αB-crystallin modulates aggregation. Hum. Mol. Genet. *14*, 2335–2347. https://doi.org/10.1093/hmg/ddi236.

26. Wang, J., Martin, E., Gonzales, V., Borchelt, D.R., and Lee, M.K. (2008). Differential regulation of small heat shock proteins in transgenic mouse models of neurodegenerative diseases. Neurobiol. Aging *29*, 586–597. https://doi.org/10.1016/j.neurobiolaging.2006.11.009.

27. Crippa, V., Sau, D., Rusmini, P., Boncoraglio, A., Onesto, E., Bolzoni, E., Galbiati, M., Fontana, E., Marino, M., Carra, S., et al. (2010). The small heat shock protein B8 (HspB8) promotes autophagic removal of misfolded proteins involved in amyotrophic lateral sclerosis (ALS). Hum. Mol. Genet. *19*, 3440–3456. https://doi.org/10.1093/hmg/ddq257.

28. Yamashita, H., Kawamata, J., Okawa, K., Kanki, R., Nakamizo, T., Hatayama, T., Yamanaka, K., Takahashi, R., and Shimohama, S. (2007). Heat-shock protein 105 interacts with and suppresses aggregation of mutant Cu/Zn superoxide dismutase: clues to a possible strategy for treating ALS. J. Neurochem. *102*, 1497–1505. https://doi.org/10.1111/j.1471-4159.2007.04534.x.

29. Chen, H.-J., Mitchell, J.C., Novoselov, S., Miller, J., Nishimura, A.L., Scotter, E.L., Vance, C.A., Cheetham, M.E., and Shaw, C.E. (2016). The heat shock response plays an important role in TDP-43 clearance: evidence for dysfunction in amyotrophic lateral sclerosis. Brain *139* (*Pt 5*), 1417–1432. https://doi.org/10.1093/brain/aww028.

30. Walters, R.W., Muhlrad, D., Garcia, J., and Parker, R. (2015). Differential effects of Ydj1 and Sis1 on Hsp70-mediated clearance of stress granules in Saccharomyces cerevisiae. RNA *21*, 1660–1671. https://doi.org/10.1261/rna.053116.115.

31. Mahboubi, H., Moujaber, O., Kodiha, M., and Stochaj, U. (2020). The Co-chaperone HspBP1 is a novel component of stress granules that regulates their formation. Cells *9*, 825. https://doi.org/10.3390/cells9040825.

32. Ganassi, M., Mateju, D., Bigi, I., Mediani, L., Poser, I., Lee, H.O., Seguin, S.J., Morelli, F.F., Vinet, J., Leo, G., et al. (2016). A surveillance function of the HSPB8-BAG3-HSP70 chaperone complex ensures stress granule integrity and dynamism. Mol. Cell *63*, 796–810. https://doi.org/10.1016/j.molcel.2016.07.021.

33. Marlin, E., Viu-Idocin, C., Arrasate, M., and Aragón, T. (2022). The role and therapeutic potential of the integrated stress response in amyotrophic lateral sclerosis. Int. J. Mol. Sci. *23*, 7823. https://doi.org/10.3390/ijms23147823.

34. Lin, J.H., Walter, P., and Yen, T.S.B. (2008). Endoplasmic reticulum stress in disease pathogenesis. Annu. Rev. Pathol. *3*, 399–425. https://doi.org/10.1146/annurev.pathmechdis.3.121806.151434.

35. Anderson, P., and Kedersha, N. (2002). Visibly stressed: the role of eIF2, TIA-1, and stress granules in protein translation. Cell Stress Chaperones *7*, 213–221. https://doi.org/10.1379/1466-1268(2002)007<0213:vstroe>2.0.co;2.

36. Pakos-Zebrucka, K., Koryga, I., Mnich, K., Ljujic, M., Samali, A., and Gorman, A.M. (2016). The integrated stress response. EMBO Rep. *17*, 1374–1395. https://doi.org/10.15252/embr.201642195.

37. López-Erauskin, J., Tadokoro, T., Baughn, M.W., Myers, B., McAlonis-Downes, M., Chillon-Marinas, C., Asiaban, J.N., Artates, J., Bui, A.T., Vetto, A.P., et al. (2018). ALS/FTD-Linked mutation in FUS suppresses intra-axonal protein synthesis and drives disease without nuclear loss-of-function of FUS. Neuron *100*, 816–830.e7. https://doi.org/10.1016/j.neuron.2018.09.044.

38. Naumann, M., Pal, A., Goswami, A., Lojewski, X., Japtok, J., Vehlow, A., Naujock, M., Günther, R., Jin, M., Stanslowsky, N., et al. (2018). Impaired DNA damage response signaling by FUS-NLS mutations leads to neurodegeneration and FUS aggregate formation. Nat. Commun. *9*, 335. https://doi.org/10.1038/s41467-017-02299-1.

39. Patel, A., Lee, H.O., Jawerth, L., Maharana, S., Jahnel, M., Hein, M.Y., Stoynov, S., Mahamid, J., Saha, S., Franzmann, T.M., et al. (2015). A liquid-to-solid phase transition of the ALS protein FUS accelerated by disease mutation. Cell *162*, 1066–1077. https://doi.org/10.1016/j.cell.2015.07.047.

40. Walters, R.W., and Parker, R. (2015). Coupling of ribostasis and proteostasis: Hsp70 proteins in mRNA metabolism. Trends Biochem. Sci. *40*, 552–559. https://doi.org/10.1016/j.tibs.2015.08.004.

41. Mateju, D., Franzmann, T.M., Patel, A., Kopach, A., Boczek, E.E., Maharana, S., Lee, H.O., Carra, S., Hyman, A.A., and Alberti, S. (2017). An aberrant phase transition of stress granules triggered by misfolded protein and prevented by chaperone function. EMBO J. *36*, 1669–1687. https://doi.org/10.15252/embj.201695957.

42. Dayalan Naidu, S., and Dinkova-Kostova, A.T. (2017). Regulation of the mammalian heat shock factor 1. FEBS J. *284*, 1606–1627. https://doi.org/10.1111/febs.13999.

43. Mathew, A., Mathur, S.K., Jolly, C., Fox, S.G., Kim, S., and Morimoto, R.I. (2001). Stress-specific activation and repression of heat shock factors 1 and 2. Mol. Cell Biol. *21*, 7163–7171. https://doi.org/10.1128/MCB.21.21.7163-7171.2001.

44. Boyault, C., Zhang, Y., Fritah, S., Caron, C., Gilquin, B., Kwon, S.H., Garrido, C., Yao, T.P., Vourc'h, C., Matthias, P., and Khochbin, S. (2007). HDAC6 controls major cell response pathways to cytotoxic accumulation of protein aggregates. Genes Dev. *21*, 2172–2181. https://doi.org/10.1101/gad.436407.

45. Pernet, L., Faure, V., Gilquin, B., Dufour-Guérin, S., Khochbin, S., and Vourc'H, C. (2014). HDAC6-ubiquitin interaction controls the duration of HSF1 activation after heat shock. Mol. Biol. Cell *25*, 4187–4194. https://doi.org/10.1091/mbc.E14-06-1032.

46. Japtok, J., Lojewski, X., Naumann, M., Klingenstein, M., Reinhardt, P., Sterneckert, J., Putz, S., Demestre, M., Boeckers, T.M., Ludolph, A.C., et al. (2015). Stepwise acquirement of hallmark neuropathology in FUS-ALS iPSC models depends on mutation type and neuronal aging. Neurobiol. Dis. *82*, 420–429. https://doi.org/10.1016/j.nbd.2015.07.017.

47. Mitchell, J.C., McGoldrick, P., Vance, C., Hortobagyi, T., Sreedharan, J., Rogelj, B., Tudor, E.L., Smith, B.N., Klasen, C., Miller, C.C.J., et al. (2013). Overexpression of human wild-type FUS causes progressive motor neuron degeneration in an age- and dose-dependent fashion. Acta Neuropathol. *125*, 273–288. https://doi.org/10.1007/s00401-012-1043-z.

48. Williamson, D.S., Borgognoni, J., Clay, A., Daniels, Z., Dokurno, P., Drysdale, M.J., Foloppe, N., Francis, G.L., Graham, C.J., Howes, R., et al. (2009). Novel adenosine-derived inhibitors of 70 kDa heat shock protein, discovered through structure-based design. J. Med. Chem. *52*, 1510–1513. https://doi.org/10.1021/jm801627a.

49. Kedersha, N., Cho, M.R., Li, W., Yacono, P.W., Chen, S., Gilks, N., Golan, D.E., and Anderson, P. (2000). Dynamic shuttling of TIA-1 accompanies the recruitment of mRNA to mammalian stress granules. J. Cell Biol. *151*, 1257–1268. https://doi.org/10.1083/jcb.151.6.1257.

50. Hetz, C., and Papa, F.R. (2018). The unfolded protein response and cell fate control. Mol. Cell *69*, 169–181. https://doi.org/10.1016/j.molcel.2017.06.017.

51. Matus, S., Valenzuela, V., Medinas, D.B., and Hetz, C. (2013). ER dysfunction and protein folding stress in ALS. Int. J. Cell Biol. *2013*, 674751. https://doi.org/10.1155/2013/674751.

52. Sidrauski, C., Acosta-Alvear, D., Khoutorsky, A., Vedantham, P., Hearn, B.R., Li, H., Gamache, K., Gallagher, C.M., Ang, K.K.H., Wilson, C., et al. (2013). Pharmacological brake-release of mRNA translation enhances cognitive memory. Elife *2*, e00498. https://doi.org/10.7554/eLife.00498.

53. Tsai, J.C., Miller-Vedam, L.E., Anand, A.A., Jaishankar, P., Nguyen, H.C., Renslo, A.R., Frost, A., and Walter, P. (2018). Structure of the nucleotide exchange factor eIF2B reveals mechanism of memory-enhancing molecule. Science *359*, eaaq0939. https://doi.org/10.1126/science.aaq0939.

54. Rabouw, H.H., Langereis, M.A., Anand, A.A., Visser, L.J., de Groot, R.J., Walter, P., and van Kuppeveld, F.J.M. (2019). Small molecule ISRIB suppresses the integrated stress response within a defined window of activation. Proc. Natl. Acad. Sci. USA *116*, 2097–2102. https://doi.org/10.1073/pnas.1815767116.

55. Sun, H., Yang, Y., Shao, H., Sun, W., Gu, M., Wang, H., Jiang, L., Qu, L., Sun, D., and Gao, Y. (2017). Sodium arsenite-induced learning and memory impairment is associated with endoplasmic reticulum stress-mediated apoptosis in rat Hippocampus. Front. Mol. Neurosci. *10*, 286. https://doi.org/10.3389/fnmol.2017.00286.

56. Elvira, R., Cha, S.J., Noh, G.-M., Kim, K., and Han, J. (2020). PERK-mediated eIF2α phosphorylation contributes to the protection of dopaminergic neurons from chronic heat stress in Drosophila. Int. J. Mol. Sci. *21*, 845. https://doi.org/10.3390/ijms21030845.

57. Cagnetta, R., Wong, H.H.-W., Frese, C.K., Mallucci, G.R., Krijgsveld, J., and Holt, C.E. (2019). Noncanonical modulation of the eIF2 pathway controls an increase in local translation during neural wiring. Mol. Cell *73*, 474–489.e5. https://doi.org/10.1016/j.molcel.2018.11.013.

58. Bounedjah, O., Desforges, B., Wu, T.D., Pioche-Durieu, C., Marco, S., Hamon, L., Curmi, P.A., Guerquin-Kern, J.L., Piétrement, O., and Pastré, D. (2014). Free mRNA in excess upon polysome dissociation is a scaffold for protein multimerization to form stress granules. Nucleic Acids Res. *42*, 8678–8691. https://doi.org/10.1093/nar/gku582.

59. Lelouard, H., Ferrand, V., Marguet, D., Bania, J., Camosseto, V., David, A., Gatti, E., and Pierre, P. (2004). Dendritic cell aggresome-like induced structures are dedicated areas for ubiquitination and storage of newly synthesized defective proteins. J. Cell Biol. *164*, 667–675. https://doi.org/10.1083/jcb.200312073.

60. Croons, V., Martinet, W., Herman, A.G., and De Meyer, G.R.Y. (2008). Differential effect of the protein synthesis inhibitors puromycin and cycloheximide on vascular smooth muscle cell viability. J. Pharmacol. Exp. Ther. *325*, 824–832. https://doi.org/10.1124/jpet.107.132944.

61. Blair, J.D., Hockemeyer, D., Doudna, J.A., Bateup, H.S., and Floor, S.N. (2017). Widespread translational remodeling during human neuronal differentiation. Cell Rep. *21*, 2005–2016. https://doi.org/10.1016/j.celrep.2017.10.095.

62. Vance, C., Scotter, E.L., Nishimura, A.L., Troakes, C., Mitchell, J.C., Kathe, C., Urwin, H., Manser, C., Miller, C.C., Hortobágyi, T., et al. (2013). ALS mutant FUS disrupts nuclear localization and sequesters wild-type FUS within cytoplasmic stress granules. Hum. Mol. Genet. *22*, 2676–2688. https://doi.org/10.1093/hmg/ddt117.

63. Bentmann, E., Neumann, M., Tahirovic, S., Rodde, R., Dormann, D., and Haass, C. (2012). Requirements for stress granule recruitment of fused in sarcoma (FUS) and TAR DNA-binding protein of 43 kDa (TDP-43). J. Biol. Chem. *287*, 23079–23094. https://doi.org/10.1074/jbc.M111.328757.

64. Daigle, J.G., Lanson, N.A., Jr., Smith, R.B., Casci, I., Maltare, A., Monaghan, J., Nichols, C.D., Kryndushkin, D., Shewmaker, F., and Pandey, U.B. (2013). RNA-binding ability of FUS regulates neurodegeneration, cytoplasmic mislocalization and incorporation into stress granules associated with FUS carrying ALS-linked mutations. Hum. Mol. Genet. *22*, 1193–1205. https://doi.org/10.1093/hmg/dds526.

65. Markmiller, S., Soltanieh, S., Server, K.L., Mak, R., Jin, W., Fang, M.Y., Luo, E.C., Krach, F., Yang, D., Sen, A., et al. (2018). Context-dependent and disease-specific diversity in protein interactions within stress granules. Cell *172*, 590–604.e13. https://doi.org/10.1016/j.cell.2017.12.032.

66. Harley, J., and Patani, R. (2020). Stress-specific spatiotemporal responses of RNA-binding proteins in human stem-cell-derived motor neurons. Int. J. Mol. Sci. *21*, 8346. https://doi.org/10.3390/ijms21218346.

67. Korobeynikov, V.A., Lyashchenko, A.K., Blanco-Redondo, B., Jafar-Nejad, P., and Shneider, N.A. (2022). Antisense oligonucleotide silencing of FUS expression as a therapeutic approach in amyotrophic lateral sclerosis. Nat. Med. *28*, 104–116. https://doi.org/10.1038/s41591-021-01615-z.

68. Weick, J.P. (2016). Functional properties of human stem cell-derived neurons in health and disease. Stem Cells Int. *2016*, 4190438. https://doi.org/10.1155/2016/4190438.

69. Hipp, M.S., Kasturi, P., and Hartl, F.U. (2019). The proteostasis network and its decline in ageing. Nat. Rev. Mol. Cell Biol. *20*, 421–435. https://doi.org/10.1038/s41580-019-0101-y.

70. Klaips, C.L., Jayaraj, G.G., and Hartl, F.U. (2018). Pathways of cellular proteostasis in aging and disease. J. Cell Biol. *217*, 51–63. https://doi.org/10.1083/jcb.201709072.

71. Li, Y., Guo, Y., Tang, J., Jiang, J., and Chen, Z. (2014). New insights into the roles of CHOP-induced apoptosis in ER stress. Acta Biochim. Biophys. Sin. *46*, 629–640. https://doi.org/10.1093/abbs/gmu048.

72. Solis, G.M., Kardakaris, R., Valentine, E.R., Bar-Peled, L., Chen, A.L., Blewett, M.M., McCormick, M.A., Williamson, J.R., Kennedy, B., Cravatt, B.F., and Petrascheck, M. (2018). Translation attenuation by minocycline enhances longevity and proteostasis in old post-stress-responsive organisms. Elife *7*, e40314. https://doi.org/10.7554/eLife.40314.

73. Hansen, M., Taubert, S., Crawford, D., Libina, N., Lee, S.-J., and Kenyon, C. (2007). Lifespan extension by conditions that inhibit translation in Caenorhabditis elegans. Aging Cell *6*, 95–110. https://doi.org/10.1111/j.1474-9726.2006.00267.x.

74. Rimal, S., Li, Y., Vartak, R., Geng, J., Tantray, I., Li, S., Huh, S., Vogel, H., Glabe, C., Grinberg, L.T., et al. (2021). Inefficient quality control of ribosome stalling during APP synthesis generates CAT-tailed species that precipitate hallmarks of Alzheimer's disease. Acta Neuropathol. Commun. *9*, 169. https://doi.org/10.1186/s40478-021-01268-6.

75. Li, S., Wu, Z., Tantray, I., Li, Y., Chen, S., Dong, J., Glynn, S., Vogel, H., Snyder, M., and Lu, B. (2020). Quality-control mechanisms targeting translationally stalled and C-terminally extended poly(GR) associated with ALS/FTD. Proc. Natl. Acad. Sci. USA *117*, 25104–25115. https://doi.org/10.1073/pnas.2005506117.

76. Wang, X., Rimal, S., Tantray, I., Geng, J., Bhurtel, S., Khaket, T.P., Li, W., Han, Z., and Lu, B. (2022). Prevention of ribosome collision-induced neuromuscular degeneration by SARS CoV-2-encoded Nsp1. Proc. Natl. Acad. Sci. USA *119*, e2202322119. https://doi.org/10.1073/pnas.2202322119.

77. Bugallo, R., Marlin, E., Baltanás, A., Toledo, E., Ferrero, R., Vinueza-Gavilanes, R., Larrea, L., Arrasate, M., and Aragón, T. (2020). Fine tuning of the unfolded protein response by ISRIB improves neuronal survival in a model of amyotrophic lateral sclerosis. Cell Death Dis. *11*, 397. https://doi.org/10.1038/s41419-020-2601-2.

78. Hosoi, T., Kakimoto, M., Tanaka, K., Nomura, J., and Ozawa, K. (2016). Unique pharmacological property of ISRIB in inhibition of Aβ-induced neuronal cell death. J. Pharmacol. Sci. *131*, 292–295. https://doi.org/10.1016/j.jphs.2016.08.003.

79. Briggs, D.I., Defensor, E., Memar Ardestani, P., Yi, B., Halpain, M., Seabrook, G., and Shamloo, M. (2017). Role of endoplasmic reticulum stress in learning and memory impairment and Alzheimer's disease-like neuropathology in the PS19 and APP(swe) mouse models of tauopathy and amyloidosis. eNeuro *4*, ENEURO.0025, 17.2017. https://doi.org/10.1523/ENEURO.0025-17.2017.

80. Zhou, Y., Liu, S., Liu, G., Oztürk, A., and Hicks, G.G. (2013). ALS-associated FUS mutations result in compromised FUS alternative splicing and autoregulation. PLoS Genet. *9*, e1003895. https://doi.org/10.1371/journal.pgen.1003895.

81. Peter, F., Trilck, M., Rabenstein, M., Rolfs, A., and Frech, M.J. (2017). Dataset in support of the generation of Niemann-Pick disease Type C1 patient-specific iPS cell lines carrying the novel NPC1 mutation c.1180T>C or the prevalent c.3182T>C mutation - analysis of pluripotency and neuronal differentiation. Data Brief *12*, 123–131. https://doi.org/10.1016/j.dib.2017.03.042.

82. Peter, F., Rost, S., Rolfs, A., and Frech, M.J. (2017). Activation of PKC triggers rescue of NPC1 patient specific iPSC derived glial cells from gliosis. Orphanet J. Rare Dis. *12*, 145. https://doi.org/10.1186/s13023-017-0697-y.

83. Carpenter, A.E., Jones, T.R., Lamprecht, M.R., Clarke, C., Kang, I.H., Friman, O., Guertin, D.A., Chang, J.H., Lindquist, R.A., Moffat, J., et al. (2006). CellProfiler: image analysis software for identifying and quantifying cell phenotypes. Genome Biol. *7*, R100. https://doi.org/10.1186/gb-2006-7-10-r100.

84. Schindelin, J., Arganda-Carrera, I., Frise, E., Kaynig, V., Longair, M., Pietzsch, T., Preibisch, S., Rueden, C., Saalfeld, S., Schmid, B., et al. (2009). Fiji - an Open platform for biological image analysis. Nat. Methods *9*, 678–682. https://doi.org/10.1038/nmeth.2019.Fiji.

85. Reinhardt, P., Glatza, M., Hemmer, K., Tsytsyura, Y., Thiel, C.S., Höing, S., Moritz, S., Parga, J.A., Wagner, L., Bruder, J.M., et al. (2013). Derivation and expansion using only small molecules of human neural progenitors for neurodegenerative disease modeling. PLoS One *8*, e59252. https://doi.org/10.1371/journal.pone.0059252.

STAR★METHODS

KEY RESOURCES TABLE

REAGENT or RESOURCE	SOURCE	IDENTIFIER
Antibodies		
Mouse anti-β-Actin	Sigma-Aldrich	Cat#A5441; RRID:AB_476744
Mouse anti-DCP1a	Abnova	Cat#H00055802-M06; RID:AB_530021
Mouse anti-EIF2a	Abcam	Cat#ab5369; RRID:AB_304838
Rabbit anti-FUS	Sigma-Aldrich	Cat#HPA008784; RRID:AB_1849181
Rabbit anti-HDAC6	Proteintech	Cat#12834-1-AP; RRID:AB_10597094
Rat anti-HSF1 (10H8)	Enzo Life Sciences	Cat#ADI-SPA-950-D; RRID:AB_2039201
Rat anti-HSF2 (3E2)	Enzo Life Sciences	Cat#ADI-SPA-960-E; RRID:AB_311836
Mouse anti-HSP27(G3.1)	Enzo Life Sciences	Cat#ADI-SPA-800-D; RRID:AB_2039215
Rabbit anti-HSP40	Enzo Life Sciences	Cat#ADI-SPA-400-D; RRID:AB_2039237
Mouse anti-HSP70/HSP72 (C92F3A-5)	Enzo Life Sciences	Cat#ADI-SPA-810; RRID:AB_10616513
Rat anti-HSP73(1B5)	Enzo Life Sciences	Cat#ADI-SPA-815-D; RRID:AB_2039279
Rabbit anti-HSP90(AC88)	Cell Signaling Technology	Cat#4874S; RRID:AB_2121214
Chicken anti-MAP2	abcam	Cat#ab5392; RRID:AB_2138153
Mouse anti-p62/SQSTM1	abcam	Cat#ab56416; RRID:AB_945626
Rabbit anti-pHSF1(EP1713Y)	abcam	Cat#ab76076; RRID:AB_1310328
Rabbit anti-Atf4 (EPR18111)	abcam	Cat#ab184909; RRID:AB_2819059
Mouse anti-Neurofilament H	Biolegend	Cat#801701; RRID:AB_2564642
Mouse anti-TIAR	BD Biosciences	Cat#610352; RRID:AB_397742
Donkey anti-Chicken IgY	Dianova GmbH	Cat#703-605-155
Donkey anti-Mouse IgG Alexa Fluor 488	Thermo Fischer Scientific	Cat#A21202; RRID:AB_141607
Donkey anti-Mouse IgG Alexa Fluor 555	Thermo Fischer Scientific	Cat#A31570; RRID:AB_2536180
Donkey anti-Rabbit IgG Alexa Fluor 488	Thermo Fischer Scientific	Cat#A21206; RRID:AB_2535792
Donkey anti-Rabbit IgG Alexa Fluor 555	Thermo Fischer Scientific	Cat#A31572; RRID:AB_162543
Donkey anti-Rat IgG Alexa Fluor 488	Dianova GmbH	Cat#712-546-150
Goat anti-Mouse IgG DyLight 680	Rockland Immunochemicals	Cat#610-144-121
Goat anti-Mouse IgG DyLight 800	Rockland Immunochemicals	Cat#610-145-003
Goat anti-Rabbit IgG DyLight 680	Rockland Immunochemicals	Cat#611-144-002
Goat anti-Rabbit IgG DyLight 800	Rockland Immunochemicals	Cat#611-145-122
Goat anti-Rat IgG DyLight 680	Rockland Immunochemicals	Cat#612-144-002
Goat anti-Rat IgG DyLight 800	Rockland Immunochemicals	Cat#612-145-002
Chemicals, peptides, and recombinant proteins		
Accutase	Sigma-Aldrich	Cat#A6964
Activin A	Biomol	Cat# 97394.10
Ascorbic Acid	Sigma-Aldrich	
B27 Supplement, w/o vitamin A	Thermo Fischer Scientific	Cat#12587010
BDNF	Peprotech	Cat# 450-02-10UG
Chiron 99021	Peprotech	Cat# 2520691
cOmplete Protease Inhibitor Cocktail Tablets	Sigma-Aldrich	Cat# 4693116001
Cycloheximide	US Biological Life Science	Cat# C8500-10
DBcAMP	Peprotech	Cat# 1698950
DMEM/F12 Medium	Thermo Fischer Scientific	Cat# 21331-020
ISRIB	Tocirs Bioscience	Cat#5284
GDNF	Peprotech	Cat# 450-10-10UG
GlutaMAX Supplement	Thermo Fischer Scientific	Cat# 35050061

(*Continued on next page*)

Continued

REAGENT or RESOURCE	SOURCE	IDENTIFIER
Laminin	Sigma-Aldrich	Cat# L2020-1MG
Matrigel Matrix	Corning Inc.	Cat# 354234
N2 Supplement	Thermo Fischer Scientific	Cat#17502-048
Neurobasal Medium	Thermo Fischer Scientific	Cat# 21103-049
Penicillin and Streptomycin	Thermo Fischer Scientific	Cat# 15140-122
PhosSTOP Phosphatase Inhibitor Tablets	Sigma-Aldrich	Cat#4906837001
Pierce™ Protein-Free (PBS) Blocking Buffer	Thermo Fischer Scientific	Cat#37572
Poly-L-Ornithine	Sigma-Aldrich	Cat#A-004-C
Purmorphamine	Biomol	Cat# 10009634
Puromycin Dihydrochloride	Thermo Fischer Scientific	Cat#540411-25MG
Retinoic Acid	Sigma-Aldrich	
RIPA Lysis and Extraction Buffer	Thermo Fischer Scientific	Cat#89901
Sodium Arsenite	Sigma-Aldrich	Cat#S7400
TGFβ-3	Peprotech	Cat# AF-100-36E-10UG
VER-155008	Sigma-Aldrich	Cat# SML0271
Critical commercial assays		
4–15% Criterion TGX Precast Midi Protein Gels	Bio-Rad Laboratories, USA	Cat#5678084
Pierce BCA Protein Assay Kit	Thermo Fischer Scientific, USA	Cat# 23225
PrestoBlue Viability Assay	Thermo Fischer Scientific, USA	Cat#A13261
Trans-Blot Turbo Midi Nitrocellulose Transfer Packs	Bio-Rad Laboratories, USA	Cat# 1704159
Experimental models: Cell lines		
Human: WT FUS-EGFP hiPSC	Naumann et al.[38]	Naumann et al.[38]
Human: P525L FUS-EGFP hiPSC	Naumann et al.[38]	Naumann et al.[38]
Human: Ctrl1 hiPSC	Naumann et al.[38]	Naumann et al.[38]
Human: Ctrl2 hiPSC	Peter et al.[81,82]	Peter et al.[81,82]
Human: R521C FUS hiPSC	Japtok et al., Naumann et al.[38,46]	Japtok et al., Naumann et al.[38,46]
Human: R521L FUS hiPSC	Naumann et al.[38]	Naumann et al.[38]
Human: R495QfsX527 FUS hiPSC	Japtok et al., Naumann et al.[38,46]	Japtok et al., Naumann et al.[38,46]
Human: FLP-293-TRex TO/FlagHA/FUS-WT	Prof. Markus Lanthaler, markus.landthaler@mdc-berlin.de	This study
Software and algorithms		
GraphPad Prism 7	GraphPad Software Inc.	https://www.graphpad.com/scientific-software/prism/
CellProfiler 2.2.0	Open source Carpenter et al.[83]	https://cellprofiler.org/
FiJi ImageJ 2.2.0-rc-65/1.52b	Open source Schindelin et al.[84]	https://imagej.net/
KNIME 3.7.2	KNIME AG	https://www.knime.com/
Image Studio Lite 5.2	LI-COR Biosciences	https://www.licor.com/bio/image-studio-lite/

RESOURCE AVAILABILITY

Lead contact

Requests for reagents or further information should be addressed to and will be fulfilled by the lead contact, Andreas Hermann (Andreas.Hermann@med.uni-rostock.de).

Materials availability

Request for FLP-293-TRex TO/FlagHA/FUS-WT cell line generated for this study will be fulfilled by the providing scientist, Prof. Dr. Markus Landthaler, markus.landthaler@mdc-berlin.de.

Requests for all other cell lines should be addressed to and will be fulfilled by the lead contact upon request.

Data and code availability

- All data reported in this paper will be shared by the lead contact upon request.
- This study does not report original code.
- Any additional information required to reanalyze the data reported in this paper is available from the lead contact upon request.

EXPERIMENTAL MODEL AND SUBJECT DETAILS

An isogenic pair of lines of hiPSC and NPC of WT FUS-EGFP and P525l FUS-EGFP which were the main cell model in this study were generated and characterized as a part of a previous study.[38] Briefly, fibroblasts of FUS R521C ALS patient (female, age at biopsy 58) were reprogrammed into hiPSC using retroviral vectors carrying cDNA of human OCT4, SOX2, KLF4 and cMYC. After establishing and characterizing the hiPSC line, CRISPR/Cas9-mediated genome editing was used to generate WT and P525L FUS-EGFP lines. This was achieved by correcting patient specific R521C mutation to WT and adding EGFP tag to the WT FUS sequence to generate WT FUS-EGFP line. In case of P525L FUS-EGFP line, the correction of R521C was accompanied by introducing P525L mutation and addition of EGFP tag to the mutated allele. All the other non-isogenic hiPSC lines used in this study were generated previously and are described in detail in Table S1. NPC maintenance and differentiation into motor neurons was based on the protocol published by Reinhardt et al.[85] In brief, NPC were maintained in the basic medium (DMEM-F12/Neurobasal 50:50 medium with N2 Supplement (1:200), B27 Supplement without vitamin A (1:100), penicillin/streptomycin (1%), GlutaMAX (1%)), supplemented with Chiron 99,021 (3 μM), Ascorbic acid (150 μM) and Purmorphamine (0.5 μM) on the dishes coated with Matrigel Matrix. For the coating, Matrigel was diluted 1:100 in DMEM-F12 and added to dishes, followed by the incubation at 37°C for 1 h. NPC were split after reaching 70–80% confluence at a 1:5–1:10 ratio using Accutase for 5 min at 37°C. For induction of the differentiation into motor neurons, NPC were split at 1:8–1:10 ratio on the Matrigel Matrix coated dish in the basic medium supplemented with BDNF (1 ng/mL), Ascorbic acid (200 μM), Retinoic acid (1 μM), GDNF (1 ng/mL) and Purmorphamine (0.5 μM) and maintained for 5 days with the medium changed every other day. For the final maturation, the medium was changed on the day 6 to the basic medium supplemented with DBcAMP (100 μM), BDNF (2 ng/mL), Ascorbic acid (200 μM), TGFβ-3 (1 ng/mL) and GDNF (2 ng/mL). Between day 7 and 10 the cells were split onto the dishes coated with Poly-L-ornithine and laminin and maintained for at least 21 days before they were used for the final analysis. The cells were regularly tested for mycoplasma contamination.

To generate FLP-293-TRex TO/FlagHA/FUS-WT cell line, commercially available Flp-In™ T-Rex™ 293 Cell Line (Invitrogen) was used according to manufacturer instructions. In short, plasmid pENTR4 FUS was generated by polymerase chain reaction (PCR) amplification. PCR was followed by restriction digest with SalI and NotI and ligation into pENTR4 (Invitrogen). pENTR4 FUS was recombined into pFRT/TO/FLAG/HA-DEST destination vector (Addgene #26361) using GATEWAY LR recombinase (Invitrogen) according to the manufacturer's protocol to allow for doxycycline-inducible expression of stably transfected FLAG/HA-tagged protein in Flp-In T-REx HEK293 cells.

The following forward (_F) and reverse (_R) primers were used for PCR and cDNA cloning into pENTR4:
FUS_F 5′-ACGCGTCGACATGGCCTCAAACGATTATACCCAAC-3′,
FUS_R 5′-ATAAGAATGCGGCCGCTCAATACGGCCTCTCCCTGCGATC-3′

The generated cells were cultured in DMEM with high glucose, l-glutamine and sodium pyruvate, supplemented with 10% FBS, 1% penicillin/streptomycin and 150 μg/mL Hygromycin B. The cells were regularly split at 1:10–1:20 ratio with 0.25% trypsin after reaching 80–90% confluence. To induce expression of FUS WT, medium was supplemented with 1 μg/mL doxycycline for up to 48 h. After that time, the cells were collected using trypsin for protein extraction or fixed and immunostained.

HeLa cells were cultured in DMEM with high glucose, l-glutamine and sodium pyruvate, supplemented with 10% FBS, 1% penicillin/streptomycin. The cells were regularly split at 1:10–1:20 ratio with 0.25% trypsin after reaching 80–90% confluence.

METHOD DETAILS

Treatments and inhibitors

To prepare stock solutions Hsp70i VER 155008 was dissolved in DMSO to the 10 mM concentration; puromycin was dissolved in water to the 1 μg/mL concentration; sodium arsenite was dissolved in water to the 200 mM concentration, ISRIB was dissolved in DMSO to the 200 μM concentration.

To induce SG formation the cells were treated with 200 μM sodium arsenite for 1 h, 40 μM Hsp70i and 2.5 μg/mL puromycin for 18 h or were incubated at 43°C in the cell culture incubator for 1 h. For the stress recovery experiments, the cells after HS were placed in the cell culture incubator at 37°C. In case of the cells treated with sodium arsenite, the medium containing arsenite was removed, cells were washed once with PBS and fresh medium with or without Hsp70i was added. The cells were fixed with ice-cold 4% paraformaldehyde immediately after the treatment and the immunofluorescence staining was performed.

To induce mild stress, the cells were treated with 50 μM sodium arsenite for 48 h, with medium change after 24 h. To inhibit ISR, the cells were treated with 200 nM ISRIB for 24 h. To block the translation, the cells were treated with either 200 μg/mL cycloheximide or with 2.5 μg/mL puromycin for up to 48 h, with the medium changed after 24 h.

Immunofluorescence staining and imaging

For the immunofluorescence staining, the cells were cultivated on the glass coverslips. The cells were fixed with 4% ice-cold paraformaldehyde for 10 min in the room temperature and next the membranes were permabilized with 0.2% Triton X-100 in PBS for 10 min in the room temperature. The unspecific binding sites were blocked with a blocking buffer (1% BSA, 5% donkey serum, 0.3 M glycine, 0.02% Triton X-100 in PBS) for 1 h in the room temperature. The primary antibodies were diluted to the desired concentration in the blocking buffer and added to the cells that were then incubated overnight at 4°C. After washing the primary antibodies solution with PBS (3 times for 5 min), the secondary antibodies dilution (1:500) in blocking buffer was applied and the cells were incubated for 1 h at the room temperature. Used antibodies are provided in the key resources table. The nuclei were stained using Hoechst (Life Technologies). The following dilution of primary antibodies were used: TIAR 1:300, MAP2 1:2000, DCP1a 1:100, FUS 1:2000.

The images were acquired with the Axiovert 200M fluorescence microscope with optical sectioning (Carl Zeiss) using 63x lens with oil immersion. The images were acquired as 6 z-stacks with the z-step of 1 μm and were later processed using FiJi ImageJ to generated maximum intensity projection. Quantification of FUS granules was performed in an automated way using CellProfiler 2.2.0. First, the nuclei were detected using Hoechst staining and the neuronal bodies were detected using MAP2 staining. The two regions were merged together to cover the whole cell region. Next, the SG were detected using TIAR staining or P-bodies were detected using DCP1a staining. FUS granules were identified based on the EGFP signal. Detected objects were then related to the MAP2 and nuclei region, to select the granules residing specifically in the neurons (FUS granules per MAP2 area). The size, shape and number of the detected objects was then measured. To analyze the co-localization, an object-based approach was applied. All the objects were first shrunk to a point and then expanded by 1 pixel. The FUS granules were then related to either SG or P-bodies and if overlap was detected, the objects were classified as co-localizing.

Quantification of FUS nuclear-to-cytosolic (N/C) ratio

The cells were immunostained as described above using FUS antibody, MAP2 antibody to detect cell bodies and Hoechst to visualize nuclei. The images were acquired using either the Axiovert 200M fluorescence microscope with optical sectioning (Carl Zeiss) or LSM 900 confocal microscope (Carl Zeiss). 63x lens with oil immersion was used. Image analysis was performed using FiJi ImageJ software. The mean fluorescence intensity of FUS antibody was measured in the nucleus and in the perinuclear cytoplasm by manual selection of the regions of interest. The measured values were then corrected for background fluorescence and used to calculate the ratio of nuclear to cytosolic FUS.

Fluorescence recovery after photo bleaching

For measuring fluorescence recovery after photo bleaching (FRAP), the neurons were seeded on the glass-bottom FluorDish (Thermo Fisher Scientific) and the FUS granules were induced prior the imaging. The imaging was performed using a spinning disc IX81 microscope with FRAPPA unit with a stage heating (37°C) and a supply of CO_2 using a 63x objective with water immersion. The region of interest including the granule was selected and photobleaching was performed using 488 nm laser at 100% power with dwell time of 50 ms repeated 3 times. The images were acquired as a single plane with 488 nm long pass filter after excitation with 488 nm laser at 12% power. 10 images at the rate of 10 frames per seconds (fps) were acquired prior to the photobleaching and 500–1000 frames at 10 fps were taken after the photobleaching. The images were analyzed with FiJi ImageJ software and a semi-automated FiJi-supported sequence of commands (macro). For each series of images, two regions of interest were selected – one region in non-photobleached area for the background correction, and one in the photobleached region. Within the photobleached region, fluorescence intensity was measured and the obtained value corrected for the background for each image was then plotted against time, generating fluorescence recovery after photo bleaching curve. The half-time recovery was automatically calculated.

Western blot

To harvest the protein, the cells were pelleted in ice-cold PBS and the protein was isolated with RIPA buffer (Thermo Fisher Scientific) supplemented with protease and phosphatase inhibitors (Sigma-Aldrich) for 40 min on ice. The samples were then centrifuged at 30,000 × g at 4°C for 20 min, and the supernatant containing the total protein fraction was collected. The protein concentration was measured with BCA assay (Thermo Fisher Scientific). SDS-PAGE was performed with the denatured samples containing 20 μg of total protein. The proteins were then transferred onto the nitrocellulose membrane (Bio-Rad Laboratories) using Trans-Blot Turbo Transfer System (Bio-Rad Laboratories). The unspecific binding sites were blocked with 5% skim milk powder (Sigma-Aldrcih) in TBS with 0.1% Tween 20 for 1 h at the room temperature with shaking. The primary antibodies dilution was prepared in 3% skim milk in TBS with 0.1% Tween 20 and applied to the membrane. The membrane was incubated overnight at 4°C with shaking. After washing off the primary antibody solution with TBS 0.1% Tween 20 (3 time for 5 min with shaking), the secondary antibodies dilution (1:10 000) was applied and the membrane was incubated for 1 h at the room temperature with shaking. Used antibodies are provided in the key resources table. After the final washing (3 times for 5 min with TBS 0.1% Tween 20, 1 time 5 min with TBS), the membrane was let to dry and was next imaged with Odyssey 9120 Fluorescent Imager (Li-Cor Biosciences). The quantitative analysis was performed using Image Studio Lite 5.2 (Li-Cor Biosciences). The following dilutions of primary antibodies were used: HSF1 1:1000, p-HSF1 1:1000, B-actin 1:10,000, HSF2 1:1000, Hsp70 1:1000, Hsp40 1:1000, Hsc70 1:1000, HDAC6 1:1000, Hsp90 1:1000, FUS 1:2000, p62 1:250, Atf4 1:1000.

Cell survival analysis

The cell viability was analyzed using PrestoBlue Viability Assay (Thermo Fisher Scientific). Briefly, the cells were incubated with the PrestoBlue reagent diluted 1:10 in the medium without phenol red for 1 h. After this time, the medium was collected and transferred into the microplate. The fluorescence was measured at 590 nm with a microplate reader and the viability was calculated in reference to the non-treated cells. Alternatively, the number of viable cells was quantified using automated cell counter and analyzer CASY (Cambridge Bioscience), which distinguishes viable and non-viable cells based on the membrane integrity. The results were normalized to non-treated control.

Filter retardation assay

The samples were prepared as for Western Blot in RIPA buffer. The protein concentration was measured using BCA assay (Thermo Fisher Scientific). To perform the filter retardation assay, a microfiltration blotting device Bio-Dot Apparatus (Bio-Rad) with cellulose acetate membrane with a pore size 0.2 μm (Merck) was used. The membrane was soaked with PBS, then with 20% methanol and finally washed once with RIPA buffer (5 min on a shaker). The membrane was placed in the apparatus on top of Whatman paper soaked in RIPA buffer and the apparatus was assembled. The wells were washed once with 200 μL RIPA buffer and then the samples containing 10 μg of protein in 100 μL of RIPA buffer were loaded. After the sample volume was filtered through, the wells were washed once more with 200 μL of RIPA buffer. The membranes was then removed from the apparatus, washed once with 20% methanol and once with TBS with 0.1% Tween 20. Next, the total protein was stained using Revert 700 Total Protein Stain (Li-Cor Biosciences) and the membrane was imaged with Odyssey 9120 Fluorescent Imager (Li-Cor Biosciences). The quantitative analysis was performed using Image Studio Lite 5.2 (Li-Cor Biosciences).

QUANTIFICATION AND STATISTICAL ANALYSIS

For all the quantitative analysis, at least 3 independent experiments based on 3 different differentiation procedures in case of neurons or 3 different passages in case of stable cell lines were performed. The statistical analysis was implemented using GraphPad Prism 7.0 software. An appropriate statistical test was chosen based on the dataset. The detailed information is provided in each figure legend. All results are reported as mean ± SEM or ±SD. The specific information is provided in each figure legend. */#$p \leq 0.05$; **/##$p \leq 0.01$; ***/###$p \leq 0.001$; ****/####$p \leq 0.0001$ were considered significant.